Topological behavior of a neutral spin-1/2 particle in a background magnetic field

B. Zygelman*
Department of Physics and Astronomy, University of Nevada, Las Vegas, Nevada 89119, USA

(Received 13 September 2020; accepted 18 March 2021; published 15 April 2021)

We present results of a numerical experiment in which a neutral spin-1/2 particle subjected to a static magnetic vortex field passes through a double slit barrier. We demonstrate that the resulting interference pattern on a detection screen exhibits fringes reminiscent of Aharonov-Bohm scattering by a magnetic flux tube. To gain better understanding of the observed behavior, we provide analytic solutions for a neutral spin-1/2 rigid planar rotor in the aforementioned magnetic field. We demonstrate how that system exhibits a generalized Aharonov-Bohm effect [Wu and Yang, Phys. Rev. D **12**, 3845 (1975)], due to the emergence of an effective SU(2) Wu-Yang (WY) flux tube. We study the behavior of the gauge invariant partition function and demonstrate a topological phase transition for the spin-1/2 planar rotor. We provide an expression for the partition function in which its dependence on the Wilson loop integral of the WY gauge potential is explicit. We generalize to a spin-1 system in order to explore the Wilczek-Zee (WZ) mechanism in a full quantum setting. We show how degeneracy is lifted by higher-order gauge corrections that alter the semiclassical WZ phase. Models that allow analytic description provide a foil to objections that question the fidelity of predictions based on the generalized Born-Oppenheimer approximation in atomic and molecular systems. Though the primary focus of this paper concerns the emergence of gauge structure in neutral systems, the theory is also applicable to systems that possess electric charge. In that case, we explore interference between fundamental gauge fields (i.e., electromagnetism) with effective gauge potentials. We propose a possible laboratory demonstration for the latter in an ion trap setting. We illustrate how effective gauge potentials influence wave-packet revivals in the said ion trap.

DOI: 10.1103/PhysRevA.103.042212

I. INTRODUCTION

The double slit experiment and the Aharonov-Bohm (AB) effect [1] are iconic examples that highlight novel and counterintuitive aspects of the quantum theory [2]. The former has long served as a pedagogical device [3] to introduce the notion of wave-particle duality to students of quantum mechanics and laboratory demonstrations of it have raised new questions regarding the role of measurement in quantum mechanics (QM) [4,5]. The AB effect demonstrates the role of gauge potentials in quantum mechanics, and Feynman [3] framed it in a double slit setting to illustrate and underscore its topological significance.

From the Einstein-Bohr-Sommerfeld quantization rules to the TKNN integers [6], topology has always played a role in QM, and for which the AB effect offers an instructive template. It has been applied to elaborate on the nature of anyons [7] and other forms of exotic quantum matter [8]. Researchers hope to harness topology in service of enabling high-fidelity qubit technology [9] and fault tolerant quantum computing [10].

In this paper we illustrate how AB-like topological effects, and their non-Abelian generalization [11,12], manifest in simple quantum systems that allow accurate numerical as well as analytic solutions. First, we consider the dynamics of a neutral spin-1/2 system coupled to an external static magnetic field. We perform a quantum-mechanical numerical experiment in which the particle passes through a double slit barrier. When the position of the particle is measured at a detection screen we find an anticipated wave interference pattern.

In addition to interference due to the presence of barrier slits, we show that the resulting pattern is best described by appealing to a model in which a charged particle is minimally coupled to the gauge potential of an effective magnetic flux tube. This, despite the fact that the spin-1/2 particle is neutral and couples locally to the external field via the standard $\vec{\mu}\cdot\vec{B}$ term.

The gauge principle forms a cornerstone to our modern understanding of the fundamental constituents of matter. Quantum electrodynamics is the best known example of an Abelian gauge theory, and its non-Abelian generalization illuminates the landscape within the nucleus. Gauge invariance guarantees charge conservation, and is the guiding principle that ensures a gauge field's raison d'être. For example, the following Hamiltonian (up to a surface term) for a scalar field ϕ,

$$\mathcal{H} = -\frac{h^2}{2m}\int d^3\boldsymbol{x}\,\phi^\dagger(\boldsymbol{x})\nabla^2\phi(\boldsymbol{x}), \tag{1}$$

is not invariant under the replacement of field operator $\phi(\boldsymbol{x})$ with $\exp[i\Lambda(\boldsymbol{x})]\phi(\boldsymbol{x})$. Introducing an auxiliary quantum field $\boldsymbol{A}$ so that

$$\mathcal{H} = -\frac{h^2}{2m}\int d^3\boldsymbol{x}\,\phi^\dagger(\boldsymbol{x})(\nabla - i\boldsymbol{A})^2\phi(\boldsymbol{x}), \tag{2}$$

*bernard@physics.unlv.edu

gauge invariance is enforced provided that, as $\phi(\boldsymbol{x}) \rightarrow \exp[i\Lambda(\boldsymbol{x})]\phi(\boldsymbol{x}), \boldsymbol{A} \rightarrow \boldsymbol{A} + \nabla\Lambda$. In QM the Schrödinger equation is not invariant under a gauge transformation of the wave amplitude, however the eigenvalues of operators, i.e., observables, are. Dirac [13] argued that a Schrödinger description in which the wave function is minimally coupled to a gauge potential is equivalent to a gauge field free theory in which wave amplitudes possess nonintegrable [11,13], or Peierls [14] phase factors.

Here we provide examples of pedestrian quantum systems in which gauge structures arise in a natural manner without the need to summon the former. This feature of QM has long been noted in studies of atomic and molecular systems [15–18]. But, as those descriptions require the application of Born-Oppenheimer (BO) like approximations, predictions are open to interpretation that attracts skepticism [19]. For example, laboratory searches for the molecular Aharonov-Bohm effect [20], in the reactive scattering of molecules, have had a long and controversial history [21–23]. In this paper we address some of those concerns in two ways: (i) we identify systems that allow analytic solutions, and (ii) we explicitly demonstrate the dependence of gauge invariant quantities (e.g., the partition function) on the Wilson loop integral of a nontrivial gauge potential. Furthermore, our analysis does not require the semiclassical notion of adiabaticity, or degeneracy in the adiabatic eigenvalues.

The numerical experiment summarized below provides a concrete demonstration of how effective gauge potentials arise in a quantum system that appear to have no overt gauge structure. This system (without the double slit) was first proposed [24] as an example of inertial frame dragging. Here we confirm, via our numerical simulation, the predictions of that gedanken system. In addition to the predicted [24] Abelian AB behavior, we explore non-Abelian features inherent in analogous systems that allow analytic solution.

In Sec. II, we summarize the results of our numerical experiment. We demonstrate the scattering of a neutral spin-1/2 wave packet by a double slit barrier. The packet experiences a background magnetic field $\vec{B}$ in which the condition $\vec{\nabla}(\vec{\mu} \cdot \vec{B}) = 0$ is satisfied. The latter ensures that the packet does not experience a gradient force. We analyze the interference pattern at a postslit detection screen and find that it shares the predicted structure of a charged particle that is scattered by an AB magnetic flux tube.

In order to gain better understanding of this phenomenon, we introduce, in Sec. III, a system that allows analytic solution. We calculate the partition function of a neutral spin-1/2 planar rotor placed in the aforementioned $\vec{B}$ field configuration. In addition to verifying the AB features observed in our numerical demonstration, we conclude that a model characterized by a Wu-Yang [11] (WY) flux tube provides a more accurate description. We demonstrate that the, gauge invariant, partition function is an explicit function of the Wilson loop [25] integral of a (WY) gauge field.

Early studies [15,16,18,26] have demonstrated how nontrivial gauge structures arise in molecular and atomic systems. In low-energy atomic collisions [18,27] and molecular structure [16] calculations, it is convenient to express the state vector in a basis of Born-Oppenheimer eigenstates. A complete set of such states leads to gauge potentials, coupled to the nuclear motion, that have both spatial and temporal components [18,27,28]. The spatial components describe a pure gauge, and it is only after truncation from a Hilbert space spanned by a complete set to a subspace that the spatial components acquire a nontrivial Wilson loop value. For that reason it has sometimes been argued that gauge fields that lead to nontrivial Wilson loop integrals (also known as geometric, or Berry, phases) are artifacts of the approximation or truncation procedure. In Sec. IV, we investigate this question for the model introduced in Sec. III. We demonstrate how an open ended, but gauge invariant, Wilson line integral of a $3+1$ gauge field along a space-time path can lead to a nontrivial spatial Wilson loop integral when projected to a closed path of the spatial subspace.

Wilzcek and Zee [29] demonstrated how non-Abelian geometric phases arise in the slow evolution of a system possessing degenerate adiabatic eigenstates that are well separated from distant states. As our spin-1/2 model contains only two internal states, separated by an energy gap, the Wilczek-Zee mechanism is not applicable. Therefore we introduce, in Sec. V, an extension to our two state model by positing a three internal state system that allows analytic solutions. In the latter, two internal states are degenerate and a third state is separated from them by a large energy defect. We analyze its gauge structure, and show that higher-order gauge corrections [17,18,27,30] break the degeneracy evident in (semiclassical) adiabatic evolution [29]. As a consequence, gauge covariance is regained only in the $3+1$ formalism [18]. In Sec. VI, we provide a summary and conclusion of our efforts and propose possible systems in which the effects described above may be gleaned in a laboratory setting.

Unless otherwise stated we use units in which $\hbar = 1$. With the exception of the Pauli matrices, we use boldface typeface to represent both vector and matrix valued quantities. In some cases, when there is the possibility of ambiguity, we use explicit vector notation to represent vector valued quantities.

II. NUMERICAL DOUBLE SLIT EXPERIMENT FOR A NEUTRAL SPIN-1/2 SYSTEM IN A STATIC MAGNETIC FIELD

Consider a neutral spin-1/2 atom or neutron with magnetic moment $\vec{\mu}$, and mass m, in the presence of a static background magnetic field

$$\vec{B} = B_t\,\hat{\boldsymbol{\phi}} + B_0\,\hat{\boldsymbol{k}} \tag{3}$$

where ϕ, ρ, z describe a cylindrical coordinate system. B_t and B_0 are taken to be constants so that $\vec{B}$ describes a vortex configuration superimposed on a constant magnetic field in the $\hat{k}$ direction. The Hamiltonian for a neutral spin-1/2 system is

$$\boldsymbol{H} = -\frac{\hbar^2}{2m}\mathbb{1}\,\vec{\nabla}^2_{\vec{R}} + \boldsymbol{V},$$
$$\boldsymbol{V} = \mu\,\boldsymbol{\sigma}\cdot\vec{B} = \begin{pmatrix} \Delta\cos\theta & -i\exp(-i\phi)\,\Delta\sin\theta \\ i\exp(i\phi)\,\Delta\sin\theta & -\Delta\cos\theta \end{pmatrix} \tag{4}$$

where μ is a constant, $\tan\theta = B_t/B_0$ is a magnetic field tilting angle and Δ is a constant. The adiabatic, or BO, eigenenergies

of $\boldsymbol{H}$ are the constant surfaces

$$V_{\rm BO} = \pm\mu\sqrt{B_t^2 + B_0^2} \equiv \pm\Delta \tag{5}$$

separated by a finite energy gap 2Δ. Though the magnetic-field lines have a vortex structure, and ignoring a small higher-order correction [28], the gradient force $-\vec{\nabla}V_{\rm BO}$ vanishes. Thus wave packets evolve, as confirmed in a previous numerical study [28], with minimal distortion induced by the presence of scalar potentials.

We use the split-operator method [31], in which the spatial coordinates are discretized into a 1024×1024 pixel grid, and wave packets obeying the time dependent Schrödinger equation

$$i\frac{\partial\psi}{\partial\tau} = -\frac{\partial^2\psi}{\partial\xi^2} - \frac{\partial^2\psi}{\partial\eta^2} + \frac{2mL^2\boldsymbol{V}}{\hbar^2}\psi. \tag{6}$$

are propagated. L is an arbitrary length scale and we have dimensionless arguments $\tau = \frac{\hbar}{2mL^2}t$, $(\xi, \eta) = (x/L, y/L)$. In this algorithm a wave packet at $t = t_0$ is propagated to $t = t_0 + \delta t$, for a small time increment δt according to

$$\psi(\tau + \delta\tau) = \boldsymbol{U}_{\rm KE}\boldsymbol{U}_V\boldsymbol{U}_{\rm KE}\,\psi(\tau) \tag{7}$$

where

$$\boldsymbol{U}_{\rm KE} = \exp\left[i\frac{\delta\tau}{2}\left(\frac{\partial^2}{\partial\xi^2} + \frac{\partial^2}{\partial\eta^2}\right)\right]\mathbb{1} \tag{8}$$

and

$$\boldsymbol{U}_V = \begin{pmatrix} \cos(\Delta\,\delta t) - i\,\cos\theta\,\sin(\Delta\,\delta t) & -\exp(-i\phi)\sin\theta\,\sin(\Delta\,\delta t) \\ \exp(i\phi)\sin\theta\,\sin(\Delta\,\delta t) & \cos(\Delta\,\delta t) + i\,\cos\theta\,\sin(\Delta\,\delta t) \end{pmatrix}\exp(-i\,V_B\delta t), \tag{9}$$

where $\phi = \phi(\xi, \eta)$. Expression (9) corresponds to exponentiation of potential matrix $\boldsymbol{V}$ modulated by V_B, the barrier potential, and $\mathbb{1}$ is a unit matrix. We follow the propagation algorithm described in detail in the Supplement to Sec. III in Ref. [32].

Figure 1 describes the evolution of a wave packet initially in the ground adiabatic state of a Zeeman split spin-1/2 system. The probability density, as a function of time, is illustrated in the panels of that figure. The system evolves on the ground-state adiabatic state, that at initial time $t = 0$ has the form

$$g(\xi, \eta) = \frac{1}{a\sqrt{2\pi}}\exp\left(-\frac{(\eta - \eta_0)^2}{a^2}\right)\exp(ik(\eta - \eta_0)) \times (\tanh(d(\xi + \xi_0)) - \tanh(d(\xi - \xi_0))) \tag{10}$$

where $a = 1/4$, $\eta_0 = -3$, $\xi_0 = 3$, $d = 4$, for the case $B_t = 0$ which corresponds to the angle $\theta = 0$ in Eq. (9). We adjusted the bias field B_0 so that the ratio of the average kinetic energy k^2 of the packet with Δ has the value $k^2/\Delta = 0.07$. Because the latter ratio is small, the packet evolves largely in its ground Zeeman state. At the detection screen, shown by the (red) dashed line, the wave amplitude forms an interference pattern that is plotted in Fig. 2. In that figure, the solid (blue) line

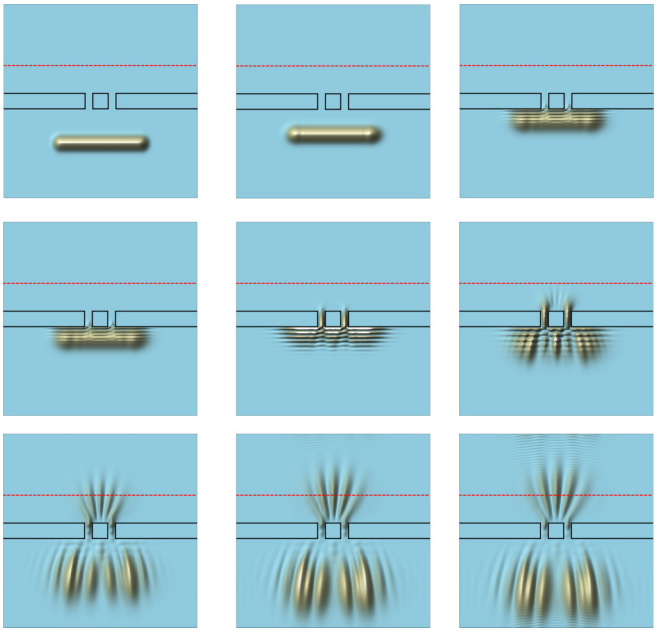

FIG. 1. Time series plot of a wave packet at initial time t_0 as it proceeds, from upper left to lower right, to a double slit barrier (solid line outline). The (red) dashed line represents a detection screen, and at final time t_f shown in the panel at the lower right the particle position is measured.

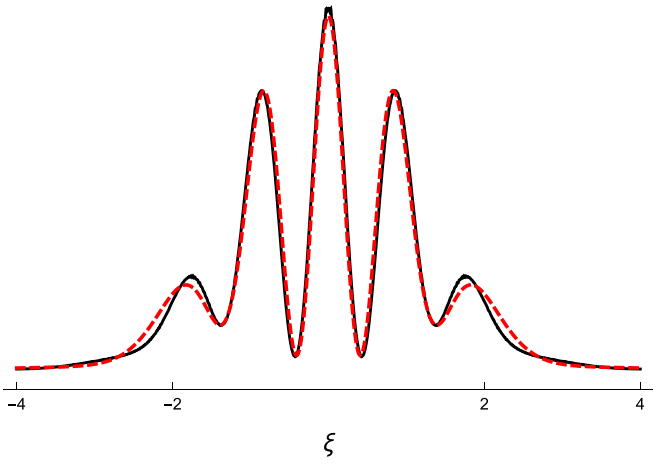

FIG. 2. Comparison of observed interference patterns at an observation screen with a fit using the model given by Eq. (11). Solid (blue) lines represent simulation data; (red) dashed lines represent a fit to Eq. (11). The horizontal axis represents the dimensionless ξ coordinate of the observation screen.

denotes the square of the absolute value of the simulated amplitude at the detection screen, whereas the (red) dashed line is an analytic fit based on a model described below. In calculating the latter we defined an effective scalar probability amplitude

$$\psi = \psi_R + \exp(i\beta)\psi_L \tag{11}$$

where $\psi_{R,L}$ are defined by the following expression:

$$\psi_{R,L}(\xi,\eta) = A\,\exp(i\kappa\,\eta)\int_{\chi_{R,L}}^{\chi_{R,L}+w}\frac{\exp(i\,\kappa\sqrt{(\eta-\eta_0)^2+(\xi-\chi)^2})}{\sqrt{(\eta-\eta_0)^2+(\xi-\chi)^2}}d\chi. \tag{12}$$

Here ξ,η are the coordinates of the observation point, $\chi_{R,L}$ are the rightmost horizontal coordinates of the right and left apertures, respectively, and w is the aperture width. The apertures are centered at $\eta = 0.5$ along a line parallel to the ξ axis, and κ, A, and β are adjustable parameters. We used the values $\kappa = 13.5, A = 11$, and $\beta = 0$ to generate the (red) dashed line in Fig. 2.

The aperture parameters $\chi_{R,L} = \{D/2, -D\}$, $w = D/2$, for $D = 1$, are fixed by the barrier geometry. Figure 2 demonstrates that model (11) with $\beta = 0$ provides a good fit to the simulated data. Modest error is localized on the outer fringes of the distribution which, presumably, can be corrected by the use of a more refined aperture function in definition (12). We define the probability distribution,

$$q(\xi) \equiv \frac{|\psi(\xi,\eta_s,t_f)|^2}{\int|\psi(\xi,\eta_s,t_f)|^2 d\xi},$$

where $\psi(\xi,\eta_s,t_f)$ is a solution to Eq. (6) at η_s, the location of the detection screen at time t_f. It is compared to a corresponding distribution $p(\xi)$, generated by the model amplitude (11). We construct a statistical measure for the similarity, or fidelity, between the two distributions, the Bhattacharyya distance [33]:

$$d_B \equiv -ln\int\sqrt{p(\xi)q(\xi)}\,d\xi. \tag{13}$$

The Bhattacharyya distance vanishes for a pair of identical distributions, and for the data shown in Fig. 2 we found the minimum value for $d_B = 0.002$, at $\beta = 0$.

In a subsequent run we adjusted the magnetic-field tilting angle so that $\theta = \pi/2$, but the value of the Zeeman energy shift was unchanged. The resulting interference pattern is illustrated in Fig. 3 by the (red) dashed line. Comparison with the results of the previous run, illustrated by the (blue) solid line, shows a dramatic shift in the pattern. A much better fit, with a Bhattacharyya distance $d_B = 0.004$, was found using the value $\beta \approx \pi$ in Eq. (11).

We also compared the probability distributions for the reflected packet on a measurement screen located behind the barrier for the two cases $\theta = 0, \theta = \pi/2$, and shown in Fig. 4. Unlike the dramatic shift in the patterns shown in Fig. 3, Fig. 4 demonstrates almost perfect alignment between the pair of interference patterns for those tilting angles.

In Table I we calculated the minimum for $d_B(\beta)$ as a function of the magnetic tilting angles θ in the range $0 \leqslant \theta \leqslant \pi$.

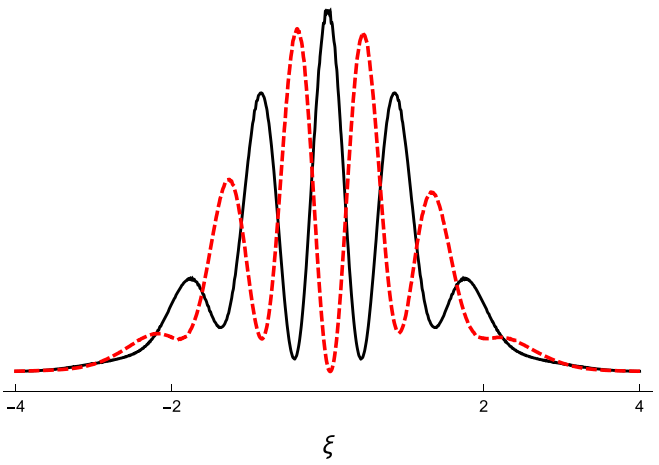

FIG. 3. Simulated data, shown by the (red) dashed line, corresponding to the magnetic tilting angle $\theta = \pi/2$. The solid (blue) line represents simulation data for the case $\theta = 0$. The horizontal axis represents the dimensionless ξ coordinate of the observation screen.

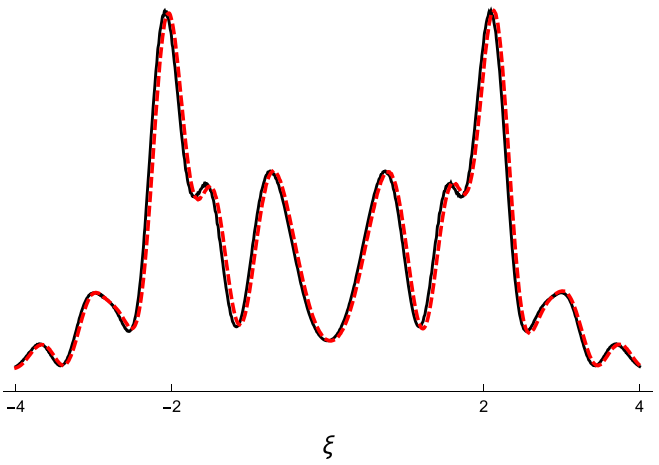

FIG. 4. Comparison of backscattered interference, for the two titling angles $\theta = 0$ [(blue) solid line] and $\theta = \pi/2$ [(red) dashed line]. The horizontal axis represents the dimensionless ξ coordinate of the observation screen.

TABLE I. The first column contains values of θ, defined in Eq. (4), that are used in the simulations. The second column itemizes $\tilde{\theta}$ for which $\beta = \pi(1-\cos\tilde{\theta})$ minimizes the Bhattacharyya distance $d_B(\beta)$. The third column itemizes the values $d_B(\beta)$. The entry for $\theta = \pi/2$ was determined by an average of two simulations obtained in different gauges.

θ	$\tilde{\theta}$	$d_B(\beta)$
0.00	0.00	0.002
0.39	0.38	0.002
0.79	0.75	0.003
1.18	1.12	0.003
1.57	1.57	0.004
1.96	2.02	0.003
2.35	2.39	0.003
2.75	2.77	0.002
3.14	3.14	0.002

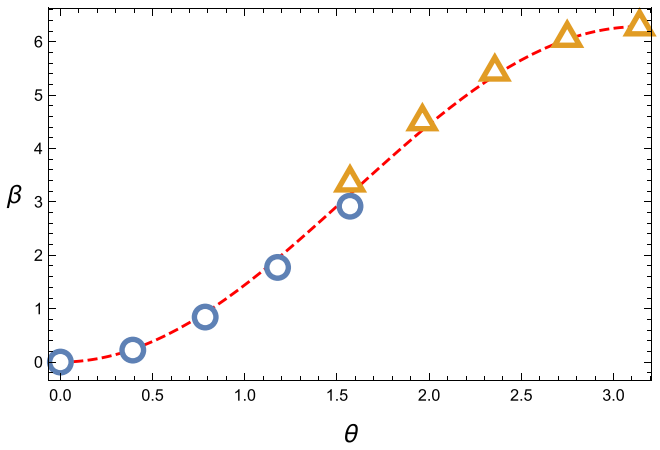

FIG. 5. Calculated values of the mixing parameter β as a function of θ obtained from the simulations. Circle icons correspond to values obtained from the propagation of an initial packet $g(\xi,\eta)$, given in Eq. (10), whereas the triangle icons represent data using the gauge transformed packet $\exp[i\phi(\xi,\eta)]g(\xi,\eta)$. The discrepancy at $\theta=\pi/2$ is attributed to Trotterization error. The dashed line denotes the theoretical values $\beta=\pi(1-\cos\theta)$.

In Fig. 5 we plot the calculated values of the mixing parameter β as a function of θ. The icons represent the values of β obtained from a time evolved wave packet that at $t=0$ is given by Eq. (10).

We also explored the behavior of the interference pattern as the vortex center ξ_c of the magnetic field is shifted from its position on the origin $\xi=0,\eta=0$, to points $\xi'>0,\eta=0$ along the barrier. In Table II we itemize the observed values for the tilting angle $\tilde{\theta}$ and the corresponding Bhattacharyya distance local minima for various values of ξ_c. In these calculations we chose $\theta=\pi/2$ and excluded values in the range $0.5<\xi_c<1$ that correspond to locations on an aperture opening.

Table II illustrates that for values $0<\xi_c<D/2$, a region obstructed by the barrier, the value for $\beta=\pi(1-\cos\tilde{\theta})\approx\pi$ is nearly constant. There is a sudden jump in β having a value consistent with a null value (Mod 2π), for values of ξ_c to the right of the aperture opening $\xi>D$. Here, the tabulated values of $\tilde{\theta}$ correspond to local minima in the Bhattacharyya distance. The global minima having values $d_\beta\approx 0.002$ are found in the range $6.0<\beta<2\pi$.

Finally, we adjust the Zeeman parameter in such a way that $\Delta/k^2\to 0$. In the extreme limit where $\Delta=0$, and the spin levels are degenerate, matrix $\boldsymbol{V}$ vanishes and each level propagates identically as a free particle, for which $\beta\to 0$. Our numerical calculations are in harmony with this prediction as $\Delta/k^2\to 0$.

TABLE II. For $\theta=\pi/2$, a tabulation for the observed values of $\tilde{\theta}$ as a function of vortex center ξ_c and $d_B(\beta)$ at their local minima. The aperture parameter $D=1$.

ξ_c	$\tilde{\theta}$	$d_B(\beta)$
0.00	1.50	0.004
$D/4$	1.49	0.004
$D/2$	1.46	0.005
D	0.00	0.009
$3D/2$	0.00	0.005
$2D$	0.00	0.004

The results are summarized by the following observations.

(1) The data obtained in the simulations, for vortex centers $-D/2<\xi_c<D/2$, are well described by Eq. (11) where β takes the value $\pi(1-\cos\theta)$.

(2) For an external magnetic field in which $|\xi_c|>|D|$ the value $\beta\approx 0$ provides a best local fit.

(3) In the region behind the barrier, in which the packet is backscattered, the interference pattern is largely insensitive to the value of the tilting angle θ.

(4) If the packet mean kinetic energy $E\gg 2\Delta$ the interference pattern is largely insensitive to the location of ξ_c and in harmony with the fit where $\beta\approx 0$.

The features described above are suggestive of dynamics influenced by topology. Indeed, it is the behavior predicted in Feynman's thought experiment treatment of AB scattering [1] of a charged scalar particle in a double slit apparatus [3]. Observations 1–4 are consistent with the following hypothesis:

$$\beta=\oint_C d\vec{s}\cdot\vec{A}\quad\text{where}\quad\vec{A}=\frac{(1-\cos\theta)}{2\rho}\hat{\boldsymbol{\phi}}\tag{14}$$

is a gauge potential that describes an AB-like flux tube of strength $(1-\cos\theta)/2$ located at the magnetic-field vortex center ξ_c within the barrier. The line integral is taken along a single circuit about a closed path C (in the counterclockwise direction) that circumscribes ξ_c.

Hamiltonian (4) possesses no overt gauge structure, but it is known [15,16,18,26] that effective gauge potentials can emerge in quantum systems not coupled to fundamental gauge fields. In this paper we highlight the utility of using a gauge theory framework to characterize quantum systems that exhibit apparent topological AB-like behavior in a scattering setting. However, the features itemized above do not completely fit into the standard AB framework. It requires, as shown below, application of non-Abelian ideas and in order to elaborate on this observation we introduce a simpler physical system that allows an analytic description.

III. A SPIN-1/2 ROTOR

We substitute the two-dimensional kinetic-energy operator, in Eq. (4), $\frac{\hbar^2}{2m}\vec{\nabla}^2_{\vec{R}}\to\frac{1}{2I}\partial^2_\phi$ (setting $\hbar=1$), so that

$$\boldsymbol{H}=-\frac{1}{2I}\mathbb{1}\,\partial^2_\phi+\mu\,\boldsymbol{\sigma}\cdot\vec{B}.\tag{15}$$

$\boldsymbol{H}$ describes a neutral spin-1/2 particle constrained on a unit circle (i.e., a planar rotor with spin and moment of inertia I), subjected to an external magnetic field given in Eq. (3). The rotor coordinates $\phi=0,2\pi$ are identified. Hamiltonian Eq. (15) can be rewritten as

$$\boldsymbol{H}=-\frac{1}{2I}\partial^2_\phi+\boldsymbol{V}\tag{16}$$

where $\boldsymbol{V}$ is defined in Eq. (4). Analytic solution to the eigenvalue problem corresponding to Hamiltonian (15) is available (see Appendix A) but, in order to gain insight, here we elicit approximate solutions to the latter. First, we transform the eigenvalue equation corresponding to Hamiltonian (15) into

the so-called adiabatic representation [18] which we define by

$$\psi = \boldsymbol{U}\, F \tag{17}$$

where

$$\boldsymbol{U} \equiv \exp(-i\sigma_3\phi/2)\exp(i\sigma_1\theta/2)\exp(i\sigma_3\phi/2) \tag{18}$$

is a single-valued unitary operator. We get

$$-\frac{1}{2I}(\partial_\phi - i\boldsymbol{A})^2 F + \Delta\,\sigma_3 F = EF \tag{19}$$

where the non-Abelian, pure, gauge potential

$$\begin{aligned}\boldsymbol{A} &= iU^\dagger \partial_\phi U \\ &= \frac{1}{2}\begin{pmatrix} \cos\theta - 1 & i\,\sin\theta\exp(-i\phi) \\ -i\,\sin\theta\exp(i\phi) & (1-\cos\theta)\end{pmatrix}.\end{aligned} \tag{20}$$

If we ignore the off-diagonal components of the gauge potential and project this equation to the ground manifold via projection operator $|-\rangle\langle -|$, we find

$$\begin{aligned}&-\frac{1}{2I}(\partial_\phi - iA_g)^2 F_g + \frac{\beta}{2I}F_g - \Delta F_g = EF_g, \\ &A_g = (1-\cos\theta)/2 \equiv \alpha, \\ &\beta = A_{12}A_{21} = (\sin^2\theta)/4 = \alpha(1-\alpha).\end{aligned} \tag{21}$$

We note that

$$F_g = \exp(im\phi) \tag{22}$$

is an eigenstate of Eq. (21) corresponding to eigenvalue

$$\begin{aligned}E_g &= \frac{(m-\alpha)^2}{2I} + \frac{(\alpha-\alpha^2)}{2I} - \Delta \\ &= \frac{m^2}{2I} - \frac{m\,\alpha}{I} + \frac{\alpha}{2I} - \Delta.\end{aligned} \tag{23}$$

It agrees with the leading-order limit of the exact analytic eigenvalue given by expression (A13) as $\Delta \to \infty$:

$$E_- = \frac{m^2}{2I} - \frac{m\,\alpha}{I} + \frac{\alpha}{2I} - \Delta = E_g. \tag{24}$$

Consider now the excited-state manifold obtained via projection $|+\rangle\langle +|$:

$$F_e = \exp(i(m-1)\phi) \tag{25}$$

is an eigenstate of the latter corresponding to eigenvalue

$$\begin{aligned}E_e &= \frac{(m-1+\alpha)^2}{2\,I} + \frac{\beta}{2I} + \Delta \\ &= \frac{m^2}{2I} + \frac{m(\alpha-1)}{I} + \frac{1-\alpha}{2I} + \Delta.\end{aligned} \tag{26}$$

Note that

$$1 - \alpha = \frac{1}{2}(1+\cos\theta)$$

and so

$$E_e = \frac{m^2}{2I} - \frac{m(1+\cos\theta)}{2I} + \frac{1+\cos\theta}{4I} + \Delta. \tag{27}$$

Comparing to Eq. (A12) we find, as $\Delta \to \infty$, $E_e \to E_+$.

In conclusion, we find that in the adiabatic gauge the approximate eigensolutions to Eqs. (19), obtained by disregarding off-diagonal couplings, are

$$\begin{aligned}\psi_g^a &= \frac{\exp(im\phi)}{\sqrt{2\pi}}\begin{pmatrix}0\\1\end{pmatrix}, \\ \psi_e^a &= \frac{\exp(i(m-1)\phi)}{\sqrt{2\pi}}\begin{pmatrix}1\\0\end{pmatrix}\end{aligned} \tag{28}$$

with eigenenergies E_g, E_e respectively. They agree with the exact analytic eigenstates of Hamiltonian (16), obtained in Appendix A, to leading order in the limit $\Delta \to \infty$.

IV. THE WU-YANG FLUX TUBE

Some time ago, Wu and Yang [11] entertained the notion of a generalized Aharonov-Bohm effect. They postulated a SU(2) flux tube that may allow, if found in nature, topological transformation of isotopic charge when a system, described by an isotopic amplitude, is transported about the flux tube. In this paper we demonstrate how the spin-1/2 system described in the previous section possesses some of the salient features of a particle, with spin degrees of freedom, coupled to a WY flux tube. To set the stage for that discussion we first introduce an idealized model in which a free rotor is coupled to a WY connection.

A. Rotor coupled to a Wu-Yang gauge potential

Consider the following gauge potential:

$$\begin{aligned}&\boldsymbol{A} = \sigma_3\vec{A} \quad \vec{A} = \{A_x, A_y\}, \\ &A_x = \frac{-\alpha\, y}{(x-x_0)^2 + y^2}, \quad A_y = \frac{\alpha\,(x-x_0)}{(x-x_0)^2 + y^2}\end{aligned} \tag{29}$$

where x, y are the coordinates of a (iso) spin-1/2 particle. It is straightforward to verify that the spatial components of the matrix-valued curvature two-form $\boldsymbol{F}$ vanish identically in the region excluding the point $x = x_0 \geqslant 0, y = 0$. From that observation it may appear that gauge connection (29) corresponds to that of a pure gauge. Nevertheless, as for the conventional AB vector potential, its Wilson loop integral circumscribing the point $x_0, y = 0$ is nontrivial.

For connection (29) the gauge invariant trace of the Wilson loop integral has the value

$$W(C) \equiv \mathrm{Tr} P \exp\left(i \oint_C d\boldsymbol{s}\cdot\boldsymbol{A}\right) = 2\cos 2\,m\,\pi\,\alpha \tag{30}$$

where C is an arbitrary contour (of counterclockwise sense) that encloses the point $(x_0, y = 0)$ and m, the winding number, itemizes the number of circuits taken around C. P represents path ordering.

As first pointed out by Wu and Yang, gauge potential (29) is an SU(2) generalization of the Aharonov-Bohm potential. As one can find a gauge in which $\boldsymbol{A}$ is diagonal and therefore has an "Abelianized" structure, the Wu-Yang gauge potential is not "truly non-Abelian" [12,16]. However, it is not simply the potential of two AB flux tubes of opposite charge [34] as $\boldsymbol{A}$ describes an SU(2) flux tube piercing the $x\,y$ plane at the point $(x_0, y = 0)$. A pictorial representation of a WY flux tube is illustrated in Fig. 6.

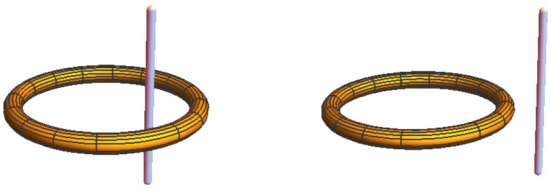

FIG. 6. Wu-Yang flux tube, piercing, or intersecting, an xy plane that is circumscribed by a rotor track (left panel). The right panel shows the flux tube exterior of the rotor track.

We seek a Schrödinger equation for a spin-1/2 particle, constrained on the unit circle $x^2 + y^2 = 1$, coupled to gauge potential (29), as well as a scalar potential $\boldsymbol{A}_0 = -\sigma_3\,\Delta$, where Δ is a constant energy defect. Constrained systems typically involve singular Lagrangians [35] and a rigorous derivation of the corresponding Hamiltonian requires application of Dirac's theory [35] of constrained dynamical systems. The latter has been applied to construct the quantum Hamiltonian of a scalar particle constrained on a circular path [36]. Here we use a more heuristic approach by considering the standard (unconstrained) Schrödinger equation in two dimensions and in which the spin-1/2 particle is minimally coupled to gauge potential (29). We have

$$-\frac{1}{2m}(\boldsymbol{\nabla} - i\boldsymbol{A})^2\psi - \boldsymbol{A}_0\psi = i\,\frac{\partial\psi}{\partial t} \tag{31}$$

where

$$\vec{A} = -\hat{r}\,\frac{\alpha\, x_0\sin(\phi)}{r^2 - 2rx_0\cos(\phi) + {x_0}^2} + \hat{\phi}\,\frac{\alpha(r - x_0\cos(\phi))}{r^2 - 2rx_0\cos(\phi) + {x_0}^2} \tag{32}$$

is expressed in a polar coordinate system. If $x_0 < r$, and in the range $-\pi < \phi \leqslant \pi$, and in which the end points are identified, the function

$$\Omega_> = \alpha\,\frac{\phi}{2} - \alpha\,\arctan\left[\frac{r + x_0}{r - x_0}\tan\left(\frac{\phi}{2}\right)\right] \tag{33}$$

is single-valued. Therefore, we are allowed the gauge transformation

$$\psi \to \psi' = \exp(-i\,\Omega_>\,\sigma_3)\psi,$$
$$\boldsymbol{A} \to \boldsymbol{A}' = \boldsymbol{A} + \nabla\Omega_> = \hat{\phi}\,\frac{\alpha}{r}. \tag{34}$$

Thus $\mathbf{A}'$ describes a WY flux tube centered at the origin. If the particle is constrained to move on the unit circle and $x_0 < 1$ we obtain the Schrödinger equation

$$\frac{1}{2I}(\partial_\phi - i\,\alpha\,\sigma_3)^2\psi' - \boldsymbol{A}_0\psi' = i\,\frac{\partial\psi'}{\partial t}. \tag{35}$$

The energy eigenstates to Eq. (35) are

$$\psi'_m(E_+) = \frac{\exp(i\,m\phi)}{\sqrt{2\pi}}\begin{pmatrix}1\\0\end{pmatrix},$$
$$E_+ = \frac{(m+\alpha)^2}{2I} + \Delta,$$
$$\psi'_m(E_-) = \frac{\exp(i\,m\phi)}{\sqrt{2\pi}}\begin{pmatrix}0\\1\end{pmatrix},$$
$$E_- = \frac{(m-\alpha)^2}{2I} - \Delta \tag{36}$$

where m is an integer.

Gauge transformation (34) using $\Omega_>$ is no longer single-valued in the region $x_0 > r$, but using

$$\Omega_< = -\alpha\,\frac{\phi}{2} - \alpha\,\arctan\left[\frac{r + x_0}{r - x_0}\tan\left(\frac{\phi}{2}\right)\right] \tag{37}$$

in Eq. (34) does induce a single-valued gauge transformation in this region. Replacing $\Omega_>$ with $\Omega_<$ in (34) we find $\mathbf{A}' = 0$, i.e., a pure gauge. Thus, for $x_0 > 1$ Eq. (35) is replaced with

$$\frac{1}{2I}\partial^2{}_\phi\psi' - \boldsymbol{A}_0\psi' = i\,\frac{\partial\psi'}{\partial t} \tag{38}$$

and

$$\psi'_m(E_+) = \frac{\exp(i\,m\phi)}{\sqrt{2\pi}}\begin{pmatrix}1\\0\end{pmatrix},$$
$$E_+ = \frac{m^2}{2I} + \Delta,$$
$$\psi'_m(E_-) = \frac{\exp(i\,m\phi)}{\sqrt{2\pi}}\begin{pmatrix}0\\1\end{pmatrix},$$
$$E_- = \frac{m^2}{2I} - \Delta. \tag{39}$$

As the position of the flux tube shifts from $x_0 < 1$ to $x_0 > 1$ the energy spectrum shifts into that of a free rotor. This topological feature is most clearly evident in the behavior of the partition function $\mathcal{Z} = \sum_m \exp(-\beta\,E_m)$ where β is an inverse temperature and E_m are the energy eigenvalues for the eigenstates summarized above. Consider the propagator for the Schrödinger Eq. (35) in the region $|x_0| < 1$ (see Appendix B, for a derivation):

$$G(\phi\,t;\phi'\,t') = \sqrt{\frac{I}{2\,\pi\,i\,\tau}}\exp(-i\sigma_3\Delta\tau)\sum_m \times \exp\left(iI\frac{(2m\pi - \phi + \phi')^2}{2\tau}\right) \times \exp(i\,\alpha(2m\pi - \phi + \phi')\,\sigma_3) \tag{40}$$

where $\tau \equiv t - t' > 0$. In this form, the propagator contains products that are proportional to the time interval τ, and are of a dynamical origin, with factors that are independent of τ and have a geometric, or topological, origin. Consider the classical equation of motion for a planar rotor $\phi(t) = \omega\,(t - t') + \phi'$ or, if we set $t' = 0$, $\phi(\tau) = \phi' + 2\,m\pi$, for a rotor trajectory that encompasses m circuits in a given time period τ. The resulting classical action

$$S_m(\tau) = \int_0^\tau dt\,\frac{I}{2}\omega^2 = I\,\frac{(\phi - \phi' - 2m\pi)^2}{2\tau} \tag{41}$$

where we used the fact that $\omega = (\phi - \phi' + 2\,m\,\pi)/\tau$. Therefore,

$$G(\phi\,t;\phi'\,t') = \sqrt{\frac{I}{2\,\pi\;i\,\tau}}\sum_m \exp(i\,S_m(\tau))\exp(-i\sigma_3\Delta\tau) \times \exp(i\sigma_3\alpha(2m\,\pi - \phi + \phi')). \tag{42}$$

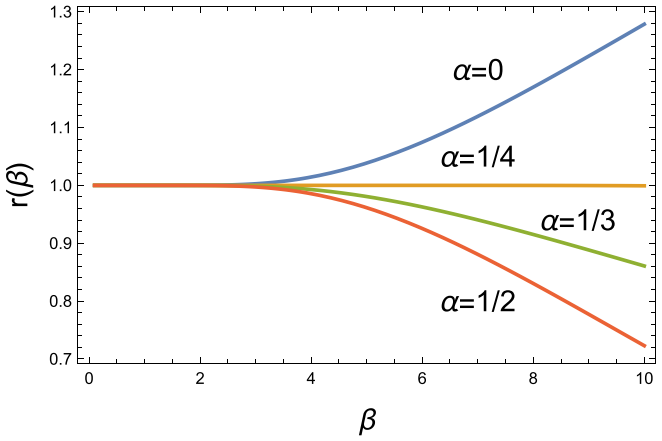

FIG. 7. Plot of the ratio $r(\beta) \equiv \mathcal{Z}_{\rm WY}/\mathcal{Z}_0$ as a function of β. The labeled curves correspond to different values of α. The parameters $I = 1$ and β are dimensionless.

The partition function corresponds to the trace over all closed paths in which $\phi = \phi'$, and the time interval τ is Wick rotated onto the imaginary axis. With the replacement $\tau \to -i\,\beta$, we obtain

$$\mathcal{Z}_{\rm WY} = \int_0^{2\pi} d\phi\, {\rm Tr}\, G(\phi, -i\,\beta, \phi, 0) = 2\sqrt{\frac{I}{2\pi\beta}}\cosh(\beta\Delta)\sum_m \exp\left(-\frac{2\pi^2 m^2 I}{\beta}\right)\cos(2m\pi\alpha). \tag{43}$$

In the same manner we construct the partition function for $x_0 > 1$. Thus, we find

$$\mathcal{Z}_{\rm WY} = \mathcal{Z}_0 \sum_m \exp\left(-\frac{2\pi^2 m^2 I}{\beta}\right)\cos(2m\pi\alpha) \quad x_0 < 1,$$
$$\mathcal{Z}_{\rm WY} = \mathcal{Z}_0 \sum_m \exp\left(-\frac{2\pi^2 m^2 I}{\beta}\right) \quad x_0 > 1,$$
$$\mathcal{Z}_0 \equiv 2\sqrt{\frac{I}{2\,\pi\,\beta}}\cosh(\beta\Delta). \tag{44}$$

In expression (44) the partition function is expressed as a product of a purely dynamical contribution $\mathcal{Z}_0$, and

$$r_{\lessgtr}(\beta) \equiv 1 + \sum_{m=1}^{\infty}\exp\left(-\frac{2\pi^2 m^2 I}{\beta}\right) 2\cos(2m\,\pi\,\alpha_{\lessgtr}), \tag{45}$$
$$\alpha_{\lessgtr} = \alpha \quad x_0 < 1, \quad \alpha_{\lessgtr} = 0 \quad x_0 > 1,$$

which is modulated by a topological term $\cos(2m\,\pi\,\alpha_{\lessgtr})$ proportional to the trace of the Wilson loop integral (30) corresponding to winding number m.

In Fig. 7 we plot the ratio $r_<(\beta)$ as a function of the inverse temperature β. The graph illustrates significant variation of that ratio with respect to α at lower temperatures.

For $x_0 > 1$, $r(\beta)$ undergoes a phase change as the curve is independent of variations in α, and reverts to that labeled by $\alpha = 0$ in that figure.

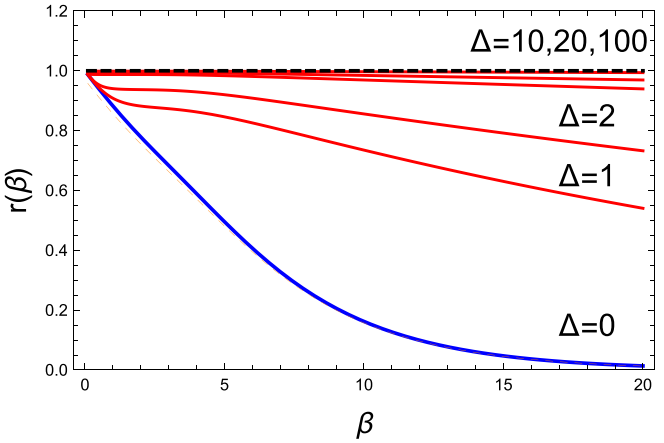

FIG. 8. Plot of the ratio $\tilde{r}(\beta)$, for different values of the energy defect Δ, as a function of β. In this graph we chose the parameter values $\alpha = 1/2, x_0 = 0, I = 1$. The ratio corresponding to the Wu-Yang system is given by the constant (black) dashed line. The (red) dashed line [superimposed by the (blue) line labeled $\Delta = 0$] corresponds to a free rotor. The parameters β and Δ are dimensionless.

Wu and Yang introduced the concept of a generalized AB effect almost 50 years ago, but, until recently, no physical system has been identified in which such an effect might be seen in the laboratory. In this paper we introduce such a system. Though non-Abelian, nonadiabatic evolution has a long history (e.g., [18,37]), below we demonstrate how the latter may exhibit effective WY gauge structure. Examples herein also allow full analytic description and address concerns that the said gauge structures are artifacts of a projection approximation.

In order to advance this thesis it is instructive to compare the behavior of the gauge invariant partition function for the Wu-Yang flux tube with that of the system described by the partition function

$$\mathcal{Z} = \sum_m \exp(-\beta E_-) + \sum_m \exp(-\beta E_+) \tag{46}$$

where $E_\pm$ are given by expression (A9). The latter correspond to the partition function of our physical model, a neutral particle constrained on a rotor track in the presence of magnetic field (3).

Instead of comparing $\mathcal{Z}_{\rm WY}$ with $\mathcal{Z}$, we compare terms that only include the topological contribution to the partition functions. To that end we define

$$\tilde{r}(\beta) \equiv \mathcal{Z}/\tilde{\mathcal{Z}}_0 \tag{47}$$

where $\tilde{\mathcal{Z}}_0$ is defined in (44) but modified by the contribution of the induced, scalar, counterterm

$$\frac{\sin^2(\theta)}{8I} = \frac{\alpha(1-\alpha)}{2I}$$

introduced in Eqs. (23) and (26), i.e.,

$$\tilde{\mathcal{Z}}_0 \equiv 2\exp\left(-\beta\frac{(\alpha-\alpha^2)}{2I}\right)\sqrt{\frac{I}{2\,\pi\,\beta}}\cosh(\beta\Delta). \tag{48}$$

In Fig. 8 we plot the ratio $r(\beta)$ for the values $\alpha = 1/2, x_0 = 0$, as a function of the inverse temperature β and the energy

defect Δ. The (blue) curve corresponding to energy defect $\Delta = 0$ is identical to the curve obtained for the partition function of a planar rotor (i.e., without nontrivial gauge couplings). Since gauge potential (20) describes a pure gauge, one might argue for the plausibility that it does not contribute to the value of the partition function $\mathcal{Z}$. However, for nonvanishing energy defects the graph shows a strong dependence of $\mathcal{Z}$ on the topological factor $\tilde{r}$. For energy defect $\Delta = 100$, the value of $\tilde{r}$ is almost identical, at low temperatures ($\beta \gg 1$), to the value predicted by the Wu-Yang flux tube given by expression (45) and shown by the dashed line in that figure. We conclude that for large values of Δ the gauge invariant partition function for the system defined in Eq. (15) approaches that of particle coupled to Wu-Yang flux tube. Though gauge potential (20) is that of a pure gauge, the energy defect Δ breaks a restricted spacial gauge symmetry as it corresponds to the time component of a $3+1$ gauge field [18]. Consequently we find a nontrivial, non-Abelian, Wilson loop contribution to the partition function. If we restrict our attention to the ground state, the latter appears as an Abelian holonomy the semiclassical analog of which [in which the quantum variable ϕ is demoted to a classical parameter $\phi(t)$] corresponds to Berry's geometric phase [38,39].

Let us define amplitude G, so that

$$\psi = \boldsymbol{U}\ \exp(-i\,\sigma_3\,\Delta\,t)G \tag{49}$$

where $\boldsymbol{U}$ is defined in Eq. (18). Inserting (49) into the time dependent version of Eq. (19), we obtain

$$-\frac{1}{2I}(\partial_\phi - i\boldsymbol{A}(t))^2 G = i\,\frac{\partial G}{\partial t} \tag{50}$$

where

$$\boldsymbol{A}(t) = \frac{1}{2}\begin{pmatrix} \cos\theta - 1 & i\,\sin\theta\exp(-i\phi(t)) \\ -i\,\sin\theta\exp(i\phi(t)) & 1-\cos\theta \end{pmatrix},$$
$$\phi(t) \equiv \phi - 2\,\Delta\,t. \tag{51}$$

$\boldsymbol{A}(t)$, like $\boldsymbol{A}$ in Eq. (20), is a pure gauge and generates a trivial Wilson loop integral. However, if we replace the off-diagonal components of (51) with a time expectation value, over interval τ,

$$\pm i\,\sin\theta\,\langle\exp(\mp i\phi(t))\rangle = \pm i\,\sin\theta\,\exp(\mp i\phi)\,\mathcal{O}\left(\frac{1}{\tau\,\Delta}\right),$$

which as $\Delta \to \infty$ we ignore. In this approximation pure gauge $\boldsymbol{A}(t)$ is replaced with the gauge potential of a SU(2) WY flux tube.

B. Shifted magnetic vortex field

In the previous section we demonstrated how, in the limit $\Delta \to \infty$, the eigensolutions to Hamiltonian (4) tend to those described by an effective Hamiltonian containing a Wu-Yang flux tube. Suppose we have the following $\vec{B}$ field configuration:

$$\vec{B}/B_0 = \frac{-y\,\hat{\boldsymbol{i}}}{\sqrt{(x-x_0)^2+y^2}} + \frac{(x-x_0)\,\hat{\boldsymbol{j}}}{\sqrt{(x-x_0)^2+y^2}}, \tag{52}$$

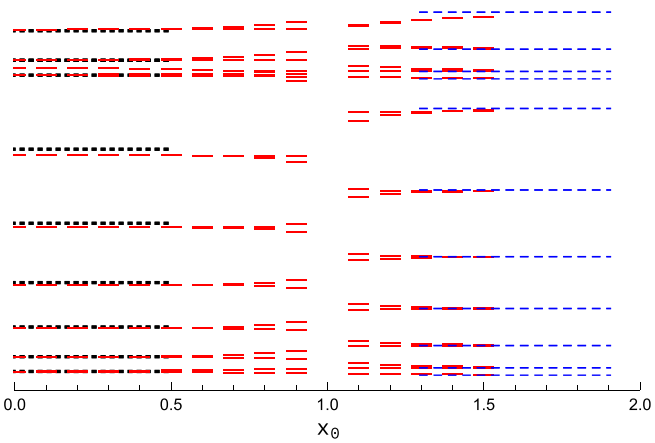

FIG. 9. Spectrum for the rotor as a function of the vortex origin. For $x_0 < 1$, it is circumscribed by the rotor track. Discontinuity at $x_0 = 1$ demonstrates evidence of a topological phase transition. Parameter x_0 is dimensionless.

which describes a vortex configuration centered at $(x = x_0, y = 0)$. The coupling term $\mu\,\boldsymbol{\sigma}\cdot\vec{B}$ is now given by

$$\begin{pmatrix} 0 & \frac{i\Delta(x_0-x+iy)}{\sqrt{(x_0-x)^2+y^2}} \\ -\frac{i\Delta(x_0-x-iy)}{\sqrt{(x_0-x)^2+y^2}} & 0 \end{pmatrix}, \quad \Delta = \mu B_0 \tag{53}$$

and replacing $x \to \cos\phi$, $y \to \sin\phi$ the above expression can be rewritten as

$$\begin{pmatrix} 0 & -i\Delta\,e^{-i\Omega(\phi)} \\ i\Delta\,e^{i\Omega(\phi)} & 0 \end{pmatrix}, \quad \tan\Omega = \frac{\sin\phi}{\cos\phi - x_0}. \tag{54}$$

Now if we define the operator

$$\boldsymbol{U} = \exp(-i\sigma_3\Omega/2)\,\exp(i\sigma_1\pi/4)\,\exp(i\sigma_3\Omega/2) \tag{55}$$

we find that

$$\boldsymbol{H} = \boldsymbol{U}\,\boldsymbol{H}_{\rm BO}\,\boldsymbol{U}^\dagger,$$
$$\boldsymbol{H}_{\rm BO} = \begin{pmatrix} \Delta & 0 \\ 0 & -\Delta \end{pmatrix}. \tag{56}$$

Forming the non-Abelian connection $\boldsymbol{A} \equiv i\boldsymbol{U}^\dagger\frac{\partial}{\partial\phi}\boldsymbol{U}$ we find

$$\boldsymbol{A} = \frac{1 - x_0\cos\phi}{2 + 2x_0^2 - 4x_0\cos\phi}\begin{pmatrix} -1 & i\,\exp(-i\Omega) \\ -i\,\exp(i\Omega) & 1 \end{pmatrix}. \tag{57}$$

The diagonal component of $\boldsymbol{A}_d$ of $\boldsymbol{A}$ has the form

$$\boldsymbol{A}_d = \sigma_3\,\frac{x_0\cos\phi - 1}{2x_0^2 - 4\cos\phi\,x_0 + 2} \tag{58}$$

and for the special case $x_0 = 0$ reduces to $\boldsymbol{A}_d = \sigma_3/2$ and describes a Wu-Yang flux tube of "charge" $1/2$ centered at the origin. In Fig. 9 we plot, with the (red) solid lines, the energy spectrum calculated for Hamiltonian (4) using field (52) for values of x_0 ranging from $x_0 = 0$ to 1.8. Superimposed on the figure, by the (blue) dotted lines, is the corresponding spectrum for a rotor system minimally coupled to the gauge field of a Wu-Yang flux tube centered at x_0, and calculated using the analytic formulas given in Eqs. (36) and (39). The

dashed (blue) lines correspond to the eigenvalues for a free planar rotor.

V. THE IMPORTANCE OF BEING NON-ABELIAN

Consider the Schrödinger equation for a spin-1/2 particle of mass m:

$$-\frac{1}{2m}(\nabla - i\vec{A}')^2\psi - A'_0(\phi)\psi = i\frac{\partial\psi}{\partial t},$$
$$A'_0(\phi) = \exp(-i\boldsymbol{a}\,\phi)\boldsymbol{\Delta}\exp(i\boldsymbol{a}\,\phi), \tag{59}$$
$$\boldsymbol{\Delta} \equiv -\Delta\,\sigma_3,$$

where $\boldsymbol{a}$ is a constant 2×2 Hermitian matrix, ϕ is the azimuthal angle in a cylindrical coordinate system, and $\vec{A}', A'_0$ are the spatial and time components of a $3+1$ matrix-valued (i.e., non-Abelian) gauge potential. Let $\vec{A}' = 0$, and so Eq. (59) describes a spin-1/2 particle coupled to a matrix, or spin-dependent, scalar potential $-A'_0$. With gauge transformation $\psi = \boldsymbol{U}F, \boldsymbol{U} = \exp(-i\boldsymbol{a}\,\phi)$, amplitude F obeys

$$-\frac{1}{2m}(\nabla - i\vec{A})^2 F - A_0(\phi)\,F = i\frac{\partial F}{\partial t} \tag{60}$$

where

$$\vec{A} = U^\dagger\vec{A}'U + iU^\dagger\nabla U = \frac{\boldsymbol{a}}{\sqrt{x^2+y^2}}\hat{\boldsymbol{\phi}},$$
$$A_0 = U^\dagger A'_0 U + iU^\dagger\frac{\partial U}{\partial t} = \boldsymbol{\Delta}. \tag{61}$$

The similarity of Eq. (59) with (60) is a reflection of the fact that the Schrödinger equation is covariant, or form invariant, with respect to gauge transformations. Observable quantities, the eigenvalues of operators, are gauge invariant.

Now gauge transformation $\boldsymbol{U}(\phi) = \exp(-i\boldsymbol{a}\,\phi)$ must be single-valued, i.e., $\boldsymbol{U}(0) = \boldsymbol{U}(2\pi)$, and so $\boldsymbol{a}$ has the form

$$\boldsymbol{a} = \boldsymbol{Z}^\dagger\begin{pmatrix} m & 0 \\ 0 & n\end{pmatrix}\boldsymbol{Z} \tag{62}$$

where m, n are integers, θ, γ are constants, and

$$\boldsymbol{Z} = \exp(i\theta\sigma_2/2)\exp(-i\gamma\sigma_3/2)$$

is a constant unitary matrix. For the sake of simplicity, we consider the case $n = -m$ and so

$$\boldsymbol{a} = q\begin{pmatrix} \cos\theta & \exp(i\gamma)\sin\theta \\ \exp(-i\gamma)\sin\theta & -\cos\theta\end{pmatrix}, \tag{63}$$

where q is an integer and θ, γ are parameters, satisfies Eq. (62). A full quantum description of this model is given in Appendix C, but here we explore the behavior of the Wilson loop integral of the $3+1$ gauge potentials $\boldsymbol{a}, \boldsymbol{A}_0$.

Consider the following path-ordered Wilson loop integral,

$$\boldsymbol{W}(C_0) = P\,\exp\left(i\oint_{C_0} d\vec{\boldsymbol{R}}\cdot\vec{\boldsymbol{A}}\right)$$
$$= \exp\left(i\boldsymbol{a}\int d\phi\right) \tag{64}$$

where we used $\vec{\boldsymbol{A}}$ defined in Eq. (61), C_0 is a closed path that circumscribes the origin in the $z = 0$, xy plane and $d\phi$ is the differential angle, with respect to the origin, of a segment of an arc along the path. Since $\int d\phi = 2\pi m$, where m is the winding number of the path,

$$\boldsymbol{W}(C_0) = \exp(i\,\boldsymbol{a}\,2\pi\,m)$$
$$= \boldsymbol{Z}^\dagger\exp(i\,2\pi\,q\,m\,\sigma_3)\,\boldsymbol{Z} = \mathbb{1}. \tag{65}$$

This identity is simply a reflection of the fact that $\vec{\boldsymbol{A}}$ is a pure gauge.

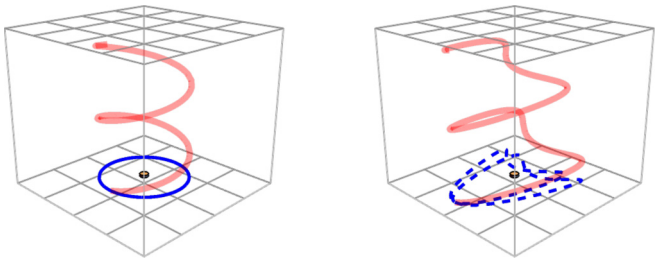

FIG. 10. Space-time paths for the Wilson line integral (66). Deformations within a set of projected paths on the xy plane, shown by the dashed lines, that share the same winding number about the origin do not alter the value of the integral. The bounding boxes provide a three-dimensional perspective for those trajectories.

A. Wilson line in space-time

In our discussion so far we noted that the partition function of our spin-1/2 system contains Wilson loop contributions that arise from nontrivial gauge fields, despite the fact that the spatial components $\vec{\boldsymbol{A}}$ of the $3+1$ gauge potentials describe a pure gauge.

To achieve a better understanding of how nontrivial Wilson loop contributions arise in systems that are putatively coupled to a pure gauge, we note that in evaluation of the partition function we need to take into account paths in space and time. Therefore, we consider a general path integral along an arbitrary path (not including the origin) $C(a,b)$ from point a to b for gauge field $\boldsymbol{A}_\mu$. Here μ is an index that identifies a space-time component

$$\boldsymbol{A}_u = \{\boldsymbol{A}_0, \boldsymbol{A}_x, \boldsymbol{A}_y, \boldsymbol{A}_z\}, \quad \mu = 0, 1, 2, 3$$

and we use a summation convention so that

$$\boldsymbol{W}(a,b) \equiv P\exp\left(i\int_{C(a,b)} dz^\mu\boldsymbol{A}_\mu\right),$$
$$dz^\mu\boldsymbol{A}_\mu \equiv dt\,\boldsymbol{A}_0 + \vec{\boldsymbol{A}}\cdot d\vec{\boldsymbol{R}}. \tag{66}$$

With gauge transformation $\psi = \boldsymbol{U}\psi'$, the gauge potentials [25]

$$\boldsymbol{A}_\nu \to \boldsymbol{A}'_\nu = \boldsymbol{U}^\dagger\boldsymbol{A}_\nu\boldsymbol{U} + i\boldsymbol{U}^\dagger\partial_\nu\boldsymbol{U}, \quad \nu = 1, 2, 3,$$
$$\boldsymbol{A}_0 \to \boldsymbol{A}'_0 = \boldsymbol{U}^\dagger\boldsymbol{A}_0\boldsymbol{U} + i\boldsymbol{U}^\dagger\partial_t\boldsymbol{U},$$
$$\boldsymbol{W}(a,b) \to \boldsymbol{U}^\dagger(b)\,\boldsymbol{W}(a,b)\,\boldsymbol{U}(a). \tag{67}$$

Consider paths of the type illustrated in Fig. 10. They are trajectories in a manifold that is a Cartesian product of the coordinates in the xy plane with a one-dimensional manifold labeled by time t. The trace of $\boldsymbol{W}(a,b)$ for an open-ended path is not, in general, gauge invariant. However, we evaluate the

integral only along paths in which the projection of coordinates a, b onto the spatial plane are equal at the initial and final points of the trajectory. We also limit the gauge group to time independent gauge transformations $\boldsymbol{U}$ so that the trace of $\boldsymbol{W}(a,b)$ is invariant under this group of transformations. Below we study the properties of $\boldsymbol{W}(a,b)$ as a function of the defect parameter Δ.

We parametrize the trajectory $z(\tau)$

$$z(\tau) = x(\tau)\hat{\boldsymbol{i}} + y(\tau)\hat{\boldsymbol{j}} + f_t(\tau)\hat{\boldsymbol{k}} \tag{68}$$

where $\hat{\boldsymbol{i}}, \hat{\boldsymbol{j}}$ are the basis vectors in the spatial plane, and $\hat{\boldsymbol{k}}$ is the unit vector orthogonal to that plane and which we take to define the time axis, so that the physical time $t \equiv f_t(\tau)$. The functions $x(\tau), y(\tau), f_t(\tau)$ are arbitrary but satisfy the conditions $x(0) = x(t_f), y(0) = y(t_f)$ where $0 < \tau \leqslant t_f$ in order for the path to make a closed loop, in the xy plane at $\tau = t_f$. Using Eqs. (61), (66), and (68) we get

$$\begin{aligned}\boldsymbol{W}(a,b) &= P\,\exp\left(i\int_{C(a,b)} dz^{\mu}\boldsymbol{A}_{\mu}\right)\\ &= T\,\exp\left(i\int_0^{t_f} d\tau\left(\frac{d\phi}{d\tau}\boldsymbol{a} + \frac{df_t}{d\tau}\boldsymbol{\Delta}\right)\right)\end{aligned} \tag{69}$$

where T denotes time ordering. If $\boldsymbol{a}$ commutes with $\boldsymbol{\Delta}$, expression (69) factors into a product of the trivial Wilson loop integral (64) and a dynamical contribution generated by $\boldsymbol{A}_0$. For gauge potential (63) such a factorization is not possible, as $[\boldsymbol{a}, \sigma_3] \neq 0$. However, integral (69) can easily be evaluated for a class of paths where $d\phi/dt \equiv \omega$ is constant. Since

$$\frac{d\phi}{dt} = \frac{d\phi}{d\tau}\frac{1}{f_t'(\tau)}$$

and $\phi(t_f) = \phi(0)\,\mathrm{Mod}(2\pi)$

$$\begin{aligned}\boldsymbol{W}(a,b) &= T\,\exp\left(i\int_0^{t_f} d\tau\,\frac{d\phi}{d\tau}\left(\boldsymbol{a} + \frac{\boldsymbol{\Delta}}{\omega}\right)\right)\\ &= \exp\left(i\,2\pi\,m\left(\boldsymbol{a} + \frac{\boldsymbol{\Delta}}{\omega}\right)\right),\end{aligned} \tag{70}$$

where m is the winding number of the path. Exponentiation of expression (70) results in

$$\begin{aligned}\boldsymbol{W}(a,b) &= \cos(2\pi m\,\Omega)\,\mathbb{1}\\ &\quad - i\frac{(\Delta/\omega - q\,\cos\theta)}{\Omega}\sin(2\pi m\,\Omega)\,\sigma_3\\ &\quad + i\frac{q\,\sin\theta}{\Omega}\,\sin(2\pi m\,\Omega)(\cos\gamma\,\sigma_1 - \sin\gamma\,\sigma_2),\end{aligned} \tag{71}$$

where

$$\Omega = \frac{\sqrt{\Delta^2 + q^2\omega^2 - 2\Delta\,q\,\omega\cos\theta}}{\omega}. \tag{72}$$

Let us define an effective vector potential

$$\vec{\mathcal{A}}_{\mathrm{eff}} \equiv \frac{\hat{\boldsymbol{\phi}}}{\sqrt{x^2+y^2}}\left(\boldsymbol{a} + \frac{\boldsymbol{\Delta}}{\omega}\right). \tag{73}$$

Unlike the pure gauge $\vec{\boldsymbol{A}}$, defined in Eq. (61), $\vec{\mathcal{A}}_{\mathrm{eff}}$ engenders a nontrivial Wilson loop integral $\mathcal{W}_C$ for any loop, in the $x\,y$ plane, enclosing the origin. Indeed,

$$\boldsymbol{W}(a,b) = \mathcal{W}_C = \oint_C d\vec{\mathbf{R}}\cdot\vec{\mathcal{A}}_{\mathrm{eff}} \tag{74}$$

where C is the projection of the space-time path (68) onto the xy plane. Because $x(0) = x(t_f), y(0) = y(t_f)$, C forms a closed loop.

In summary, we demonstrated how the space-time open-ended path integral of a $3+1$ non-Abelian gauge potential leads to a nontrivial Wilson loop integral of an effective gauge field $\vec{\mathcal{A}}_{\mathrm{eff}}$. For time independent gauge transformations, the trace of $\boldsymbol{W}$ is gauge invariant. As $\mathcal{W}_C$ depends only on the winding number, C can be shrunk to an infinitesimal loop about the origin without altering the value of $\mathcal{W}_C$. Thus $\vec{\mathcal{A}}$ represents the gauge potential of a Wu-Yang flux tube of "charge" $\pm\Omega$, the eigenvalues of $\boldsymbol{a} + \frac{\boldsymbol{\Delta}}{\omega}$. In general, $\boldsymbol{W}(a,b)$ is a function of the dynamical parameters, Δ, $\boldsymbol{\omega}$, but for large $\frac{\Delta}{\omega} \gg 1$ it tends to the product

$$\begin{aligned}\boldsymbol{W}(a,b) &= \exp\left(-\frac{2\,i\,m\pi\,\Delta}{\omega}\,\sigma_3\right)\exp(2\,i\,m\,\pi\,q\,\cos\theta\,\sigma_3)\\ &\quad + \mathcal{O}(\omega/\Delta).\end{aligned} \tag{75}$$

We evaluated $\boldsymbol{W}$ in the adiabatic gauge [18], wherein $\boldsymbol{A}_0$ is diagonal. Because $\boldsymbol{U}(\phi = 0) = \boldsymbol{U}(\phi = 2\pi) = \mathbb{1}$, $\boldsymbol{W}$ is invariant under a gauge transformation into the diabatic gauge [18]. The latter corresponds to Schrödinger Eq. (59) in which the spatial component $\vec{\boldsymbol{A}}' = 0$. In that gauge

$$\begin{aligned}\boldsymbol{W}(a,b) &= P\,\exp\left(i\int_{C(a,b)} dz^{\mu}\boldsymbol{A}'_{\mu}\right)\\ &= T\,\exp\left(i\int_0^{t_f} d\tau\,\frac{df_t}{d\tau}\boldsymbol{A}'_0(\phi(\tau))\right)\\ &= T\,\exp\left(i\int_0^{\frac{2\pi m}{\omega}} dt\,\exp(-i\boldsymbol{a}\,\omega\,t)\boldsymbol{\Delta}\exp(i\boldsymbol{a}\,\omega\,t)\right)\end{aligned} \tag{76}$$

where we used the fact that $f_t(\tau) = t$ and $\phi(t) = \omega t$. Replacing the upper limit in integral (76) with an arbitrary time value t, we find that $\boldsymbol{W}(t)$ obeys a time dependent Schrödinger equation:

$$\begin{aligned}-i\,\dot{\boldsymbol{W}}(t) &= \mathcal{H}(t)\,\boldsymbol{W}(t),\\ \mathcal{H}(t) &= \exp(-i\boldsymbol{a}\,\omega\,t)\boldsymbol{\Delta}\exp(i\boldsymbol{a}\,\omega\,t).\end{aligned} \tag{77}$$

It can be integrated to give

$$\boldsymbol{W}(t) = \exp(-i\,\boldsymbol{a}\,\omega\,t)\exp\left(i\,\omega\,t\left(\boldsymbol{a} + \frac{\boldsymbol{\Delta}}{\omega}\right)\right). \tag{78}$$

Thus,

$$\boldsymbol{W}(a,b) = \boldsymbol{W}\left(t = \frac{2\pi m}{\omega}\right)$$

where we used the fact that $\exp(2\,i\,\pi\,m\,\boldsymbol{a}) = \mathbb{1}$. In the adiabatic limit as $\omega \to 0$, $\boldsymbol{W}(a,b)$ tends to the limit Eq. (75). In that expression, the first, dynamical, factor $\exp(-\frac{2\,i\,m\pi\,\Delta}{\omega}\,\sigma_3)$ depends on the length of time $t_f = 2\pi m/\omega$ that it takes for the system to travel from starting to end points. The second

factor

$$\exp(2\,i\,m\,\pi\,q\,\cos\theta\,\sigma_3)$$

depends on the spatial path taken. This factorization is in harmony with the adiabatic theorem [38].

VI. ON THE WILCZEK-ZEE MECHANISM

In the previous sections we illustrated how nontrivial gauge structures arise in a vector space that is a direct product of a two state (or qubit) system with the Hilbert space of a rotor. It is straightforward to extend this formalism to systems possessing additional internal degrees of freedom (e.g., spin-1, etc.). Indeed, this procedure is ubiquitous in theoretical studies of slow atomic collisions and nonadiabatic molecular dynamics. In those applications it is especially applicable if the total system energy $E \ll \Delta$ where Δ is an energy defect that separates a submanifold of BO states separated by a large energy gap from energetically higher-lying BO states. Thus the Hilbert-space amplitude is projected to a set of effective, or matrix-valued, amplitudes in the subspace. The resulting set of coupled equations constitutes the Born-Huang [40] approximation, or the method of perturbed stationary states [41] (PSS). The latter typically result in effective, nontrivial, non-Abelian gauge couplings among the subspace amplitudes.

In a quasiclassical version of this procedure, Wilczek and Zee demonstrated how the projected amplitudes, for a submanifold of degenerate energy eigenstates, acquire a non-Abelian geometric phase during adiabatic evolution.

Below we consider a spin-1 rotor system in which two internal states possess degenerate energy eigenvalues that are separated from the remaining internal states by a large energy gap Δ. To illustrate this mechanism we choose a straightforward extension of Hamiltonian (59):

$$\begin{aligned} H &= -\frac{1}{2\,I}\partial_\phi^2 + \boldsymbol{U}(\phi)\boldsymbol{V}\boldsymbol{U}^\dagger(\phi), \\ \boldsymbol{U} &= \exp(-i\,\boldsymbol{a}\,\phi), \\ \boldsymbol{a} &= \begin{pmatrix} 0 & \frac{\sin\theta}{\sqrt{2}} & -\frac{\sin\theta}{\sqrt{2}} \\ \frac{\sin\theta}{\sqrt{2}} & \cos\theta & 0 \\ -\frac{\sin\theta}{\sqrt{2}} & 0 & -\cos\theta \end{pmatrix}, \\ \boldsymbol{V} &= \begin{pmatrix} \Delta & 0 & 0 \\ 0 & e_g & 0 \\ 0 & 0 & e_g \end{pmatrix}. \end{aligned} \tag{79}$$

This particular choice for $\boldsymbol{a}$ guarantees that $\boldsymbol{U}$ is single-valued. For our purposes it is convenient to choose $e_g = -\sin^2\theta/4I$.

Defining the adiabatic gauge amplitude F, so that

$$\psi = \boldsymbol{U}\,F$$

we obtain the matrix-valued Schrödinger equation

$$-\frac{1}{2I}(\partial_\phi - i\,\boldsymbol{a})^2\,F + \boldsymbol{V}\,F = i\frac{\partial F}{\partial t}. \tag{80}$$

With ansatz

$$F = \exp(im\phi)\exp(-i\,E\,t)\,\boldsymbol{c} \tag{81}$$

where $\boldsymbol{c}$ is a constant column matrix, we are led to the eigenvalue equation $\det|\boldsymbol{h} - \mathbb{1}\,E| = 0$ where

$$\boldsymbol{h} = \frac{(\mathbb{1}\,m - \boldsymbol{a})^2}{2\,I} + \boldsymbol{V}. \tag{82}$$

Finding the eigenvalues of $\boldsymbol{h}$ involves solving for the roots of a cubic equation, and for analytic expressions the Cardano formula is available. The latter can be used to construct the gauge invariant partition function

$$\mathcal{Z} \equiv \sum_{i=1}^{3}\sum_m \exp\left(-\beta\,E_m^i\right) \tag{83}$$

to the required degree of accuracy. The sums extend over the spectrum of $\boldsymbol{h}$, which are itemized by the motional quantum number m, as well as the internal state quantum number i. Here β is an inverse temperature.

Instead, because $\Delta \gg e_g$, we use the PSS approximation in which the amplitude F is projected to a Hilbert subspace. In this case, the subspace is spanned by the degenerate eigenstates of $\boldsymbol{V}$, or the computational basis for a single qubit. Introducing the projection operator

$$P \equiv \begin{pmatrix} 0 & 0 & 0 \\ 0 & 1 & 0 \\ 0 & 0 & 1 \end{pmatrix}$$

defining

$$G = P\,F$$

we obtain the PSS equations

$$-\frac{1}{2I}(\partial_\phi - i\,\boldsymbol{a}_p)^2\,G + P\,\frac{\boldsymbol{a}\cdot\boldsymbol{a} - \boldsymbol{a}_p\cdot\boldsymbol{a}_p}{2I}\,G + \boldsymbol{V}_p\,G = i\frac{\partial G}{\partial t} \tag{84}$$

where $\boldsymbol{a}_p \equiv P\boldsymbol{a}P$, $\boldsymbol{V}_p = P\,\boldsymbol{V}\,P$. In this approximation we ignore couplings between the P and $Q = \mathbb{1} - P$ submanifolds.

Though $\boldsymbol{V}_p$ is diagonal and degenerate, the higher-order induced scalar term [17,27]

$$P\,\frac{\boldsymbol{a}\cdot\boldsymbol{a} - \boldsymbol{a}_p\cdot\boldsymbol{a}_p}{2I}\,P = \frac{1}{4I}\begin{pmatrix} 0 & 0 & 0 \\ 0 & \sin^2\theta & -\sin^2\theta \\ 0 & -\sin^2\theta & \sin^2\theta \end{pmatrix} \tag{85}$$

is not. An additional gauge transformation in the projected qubit subspace $G = \boldsymbol{W}G'$ results in

$$\begin{aligned} &-\frac{1}{2I}(\partial_\phi - i\,\boldsymbol{a}'_p)^2\,G' + \boldsymbol{V}'_p\,G' = i\frac{\partial G'}{\partial t}, \\ &\boldsymbol{a}'_p = \cos\theta\,\sigma_1, \\ &\boldsymbol{V}'_p = \frac{\sin^2\theta}{4I}\,\sigma_3, \\ &\boldsymbol{W} = \exp(i\sigma_2\pi/4) \end{aligned} \tag{86}$$

where σ_i are the standard spin-1/2 Pauli matrices.

Because the eigenstates of $\boldsymbol{V}'_p$ are not degenerate, Eq. (86) is no longer covariant under a Wilczek-Zee gauge transformation. In the latter formulation $\phi(t)$ is treated as a classical variable undergoing adiabatic evolution. Here ϕ is a quantum variable, and the symmetry responsible for the degeneracy in a quasiclassical formulation is broken. However we can, as

described in the previous sections, enlarge the gauge group by allowing the (matrix) scalar potential to be treated as the time component of a $3+1$ gauge potential.

Consider the gauge potential:

$$\boldsymbol{A}'_p = \sigma_1 \cos\theta \left(\frac{-\hat{\boldsymbol{i}}\, y}{x^2+y^2} + \frac{\hat{\boldsymbol{j}}\, x}{x^2+y^2} \right), \tag{87}$$

which begets $\mathbf{a}'_p$ in the constrained rotor system described in Eq. (86). Its Wilson loop integral for a path C circumscribing the origin assumes the value

$$\begin{aligned} \mathcal{W}_C(m) &\equiv \mathrm{Tr}\, P \exp\left(i \oint_C d\boldsymbol{r} \cdot \boldsymbol{A}'_p \right) \\ &= 2\cos(2\pi\, m\, \cos\theta) \end{aligned} \tag{88}$$

where m is the winding number. For values $\cos\theta \notin \mathbb{Z}$, identity (88) demonstrates that $\boldsymbol{a}'_p$, unlike $\boldsymbol{a}$ in Eq. (62), is not a pure gauge. The energy eigenvalues associated with Eq. (86) are

$$\begin{aligned} E &= e_0 \pm e_1, \quad e_0 = \frac{m^2 + \cos^2\theta}{2\,I}, \\ e_1 &= \frac{1}{I}\sqrt{\frac{\sin^4\theta}{16} + m^2\, \cos^2\theta} \end{aligned} \tag{89}$$

and so the reduced partition function

$$z = 2\sum_m \exp(-\beta\, e_0)\cosh(\beta\, e_1). \tag{90}$$

For higher temperatures, or $\beta \ll 1$, we can approximate

$$e_1 \approx \frac{|m\cos\theta|}{I},$$

which implies that

$$z \approx 2\sum_m \exp\left(-\beta\, \frac{m^2+\cos^2\theta}{2\,I} \right) \cosh\left(\beta\, \frac{m\, \cos\theta}{I} \right). \tag{91}$$

Applying the Poisson summation formula, we get

$$z \approx 2\sqrt{\frac{2\pi\, I}{\beta}} \sum_m \exp\left(-\frac{2\,I\, m^2\pi^2}{\beta} \right) \cos(2\pi\, m\, \cos\theta). \tag{92}$$

In order to obtain the total partition function $\mathcal{Z}$, we must include the contribution from the distant state with energy eigenvalue $E_m^{i=1} \gg e_0 \pm e_1$. In solving for the eigenvalues of $\boldsymbol{h}$ we find that

$$E_m^{i=1} = \frac{m^2}{2\,I} + \frac{\sin^2\theta/2}{2\,I} + \Delta + \mathcal{O}\left(\frac{1}{\Delta}\right) + \ldots \tag{93}$$

and so the leading-order contribution is dominated by the term $\exp(-\beta\,\Delta) \to 0$ as $\Delta \to \infty$. Therefore,

$$\mathcal{Z} \approx z = \sqrt{\frac{2\pi\, I}{\beta}} \sum_k \exp(-S_0(k))\cos(\mathcal{W}_C(k)) \tag{94}$$

where $S_0(k) = 2\pi^2 k^2 I/\beta$ is proportional to the Wick rotated classical action for a free rotor making k complete circuits in a given time interval. It contains a dynamical contribution, proportional to the classical action, that is modulated by a purely topological term, the Wilson loop integral $\mathcal{W}_C(k)$. At higher temperatures z is largely dominated by contributions from the classical action and so we investigate the behavior of $\mathcal{Z}$ in the low-temperature $\beta \to \infty$ limit. A detailed derivation is given in Appendix D and according to Eqs. (D12)

$$\begin{aligned} z \to\ & 2\sqrt{\frac{2\,\pi\, I}{\beta}}\, \exp(\beta\, V(\theta)) \\ & \times \sum_k \exp(-S_0(k))\cos(2\,\pi\, k\, \Omega) \end{aligned} \tag{95}$$

in that limit.

$$\begin{aligned} V(\theta) &= -\frac{\cos^2\theta}{I} + \alpha_0 + \frac{I\,{\alpha_1}^2}{2}, \\ \Omega &= -\frac{\sin^2\theta}{4} + \sqrt{\frac{\sin^2\theta}{16} + \cos^2\theta} \end{aligned} \tag{96}$$

where α_0, α_1 are defined in Eq. (D2). In Fig. 9 we plot

$$E_g = \lim_{\beta\to\infty} F(\beta) \tag{97}$$

where $F = -\ln z/\beta$ is the Helmholtz free energy, and which in the limit $\beta \to \infty$ represents the ground-state energy. In Fig. 11, the solid line denotes the ground-state energy for Hamiltonian (79), the dashed line denotes the adiabatic energy e_g, and the circle icons denote energies obtained in the PSS approximation and calculated using expression (95) for the partition function. The latter approximation is accurate for values $\Delta/e_g \gg 1$. According to expression (95), the term $k\,\Omega$ is independent of the temperature parameter β and is therefore of topological origin. The cross icons in that figure represent the energies obtained by artificially setting $\Omega = 0$ in expression (95). The difference between those values and the ones laying on the solid line, underscores the significance of that topological contribution. Interestingly, unlike in the high-temperature limit, the value for $2\pi\, k\, \Omega$ does not equal the Wilson loop integral $\mathcal{W}_C$ of the projected gauge potential $\boldsymbol{A}'_p$.

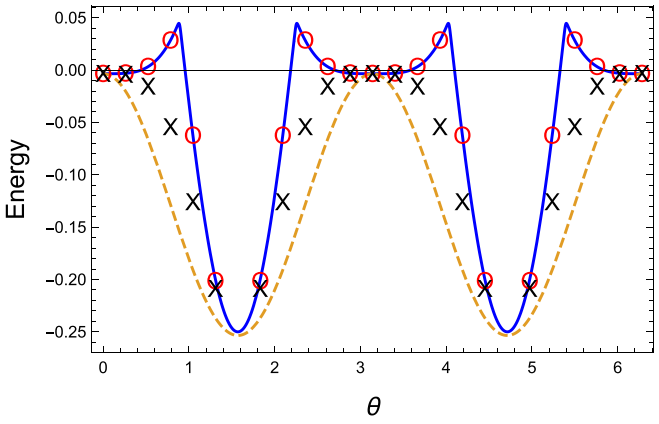

FIG. 11. Ground-state (dimensionless) energy of Hamiltonian (79) as a function of gauge parameter θ.

VII. CONCLUSION

In the remaining discussion we address possible laboratory demonstrations of effects predicted and discussed in this paper. Though we are unable to comment on the viability of

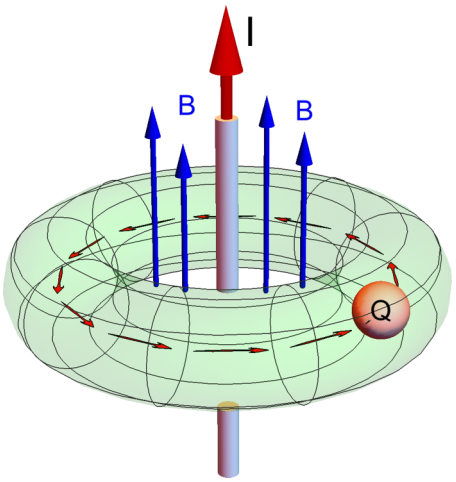

FIG. 12. Illustration of a toroidal trap in which an ion of charge Q simulates the motion of a planar, quasirigid, rotor. A current I [(red) arrow] threading the doughnut hole induces an axial magnetic field. The system is subjected to a background magnetic bias field (blue) arrow.

present day laboratory capabilities to realize the double slit system discussed in the introduction, we anchor our focus on recent laboratory efforts to simulate a coherent quantum rotor. For example, a planar quantum rotor was simulated [42] in a cylindrical symmetric ion trap in which a pair of $^{40}Ca^{+}$ ions formed a two-ion Coulomb crystal. That experiment demonstrated a capability to prepare and control angular momentum states. Along those lines we propose trapping a spin-1/2 ion in a toroidal trap as shown in Fig. 12. In that figure a positively charged spin-1/2 ion, such as Ca^{+} in its ground state, is trapped in the torus. Instead, one can also consider a pair of ions forming a Coulomb crystal, as described in [42]. The latter simulates, after factoring out the center-of-mass motions, a single ion rotor. However, for the sake of illustration, we limit this discussion to a toroidal trap configuration.

We thread an electric current along the symmetry axis piercing the doughnut hole to induce a magnetic field along the axial direction of the torus. Alternatively, an axial magnetic field can also be generated by joining a solenoid at its ends to form a torus (i.e., a microtokamak). In addition to the toroidal axial field, generated by current I, a constant homogeneous bias magnetic field of magnitude B_0 parallel to the symmetry axis is applied. The Hamiltonian for this system is

$$\boldsymbol{H} = \frac{-\hbar^2}{2m}\left(\nabla\mathbb{1} - i\frac{q}{\hbar c}\boldsymbol{A}_0\right)^2 + \boldsymbol{U}(\phi)\boldsymbol{\Delta}(\rho)\boldsymbol{U}^{\dagger}(\phi) + V_{\rm trap} \quad (98)$$

where, in a cylindrical coordinate system,

$$\boldsymbol{A}_0 = \left(\hat{\boldsymbol{\phi}}\,\frac{B_0\,\rho}{2} - \hat{z}\,\frac{\mu_0 I}{2\pi}\ln\rho\right)\mathbb{1} \quad (99)$$

is the Landau gauge vector potential for the total magnetic field. $\boldsymbol{U}(\phi)$ is given by Eq. (18),

$$\cos\theta = \frac{B_0}{\sqrt{{B_0}^2 + \left(\frac{u_0 I}{2\pi\rho}\right)^2}},$$

q is the charge of the ion, μ_0 is the magnetic constant,

$$\boldsymbol{\Delta}(\rho) = \mu\sqrt{B_0^2 + \left(\frac{I\mu_0}{2\pi\,\rho}\right)^2}\,\sigma_3,$$

and $V_{\rm trap}$ is a trapping potential.

In the adiabatic representation, and assuming that $V_{\rm trap}$ is independent of spin, we obtain the eigenvalue Schrödinger equation:

$$\frac{-\hbar^2}{2m}(\nabla - i\mathcal{A})^2 F(\mathbf{r}) + \boldsymbol{\Delta}(\rho)F(\mathbf{r}) + V_{\rm trap}(\mathbf{r})F(\mathbf{r}) = EF(\mathbf{r}), \quad (100)$$

where

$$\begin{aligned}\mathcal{A} &= i\boldsymbol{U}^{\dagger}\nabla\boldsymbol{U} + \boldsymbol{A}_0\\ &= \frac{\hat{\boldsymbol{\phi}}}{2\rho}\begin{pmatrix}\cos\theta - 1 + \frac{q}{\hbar c}B_0\rho^2 & i\,\sin\theta\exp(-i\phi)\\ -i\,\sin\theta\exp(i\phi) & (1-\cos\theta) + \frac{q}{\hbar c}B_0\rho^2\end{pmatrix}\\ &\quad + \hat{\boldsymbol{\rho}}\begin{pmatrix}0 & -\frac{1}{2}\exp(-i\phi)\theta'(\rho)\\ -\frac{1}{2}\exp(i\phi)\theta'(\rho) & 0\end{pmatrix}\\ &\quad - \hat{z}\,\frac{q\,\mu_0 I}{2\,\hbar\,c\,\pi}\ln\rho\begin{pmatrix}1 & 0\\ 0 & 1\end{pmatrix}.\end{aligned} \quad (101)$$

Assuming that the trap potential is effective in freezing the degrees of freedom in the radial and $\hat{z}$ direction, and for a large Zeeman energy gap Δ, we replace the three-dimensional Schrödinger Eq. (100) with an effective one-dimensional equation corresponding to a rigid planar rotor:

$$\begin{aligned}&\frac{-\hbar^2}{2m\rho_0^2}(\partial_\phi - i\mathcal{A}_{\rm eff})^2 F(\phi) + \boldsymbol{\Delta}(\rho_0)F(\phi) = E\,F(\phi),\\ &\mathcal{A}_{\rm eff} = \frac{1}{2}\begin{pmatrix}\cos\theta(\rho_0) - 1 + \frac{q\Phi}{\hbar\pi\,c} & 0\\ 0 & 1 - \cos\theta(\rho_0) + \frac{q\Phi}{\hbar\pi\,c}\end{pmatrix}\end{aligned} \quad (102)$$

where ρ_0 is the equilibrium value of the radial coordinate, and $\Phi = B_0\pi{\rho_0}^2$ is the total magnetic flux enclosed by the rotor. By tuning the current I and the bias field B_0 we can alter and discriminate the values of the Wilson loop for different spin states. For example, if

$$\cos\theta(\rho_0) - 1 + \frac{q\Phi}{\hbar\pi c} = 0$$

then

$$\mathcal{A}_{\rm eff} \to \begin{pmatrix}0 & 0\\ 0 & \frac{q\Phi}{\hbar\pi\,c}\end{pmatrix}. \quad (103)$$

In this scenario the upper Zeeman level undergoes the motion of a free rotor, whereas the lower component experiences an effective AB flux tube with charge Φ. Such a capability, if realized, could find application as a different type of magnetometer and rotational sensor.

The planar rotor has also been used as a model for the anyon [7]. In adiabatic transport about a flux tube it can acquire a noninteger phase (modulus 2π) as it completes one circuit. In the rotor systems discussed here adiabatic transport is problematic as an initial wave packet spreads in time. However, as a closed system, it eventually revives to its original

shape. For example, the propagator for a spin-1/2 planar rotor coupled to a Wu-Yang flux tube of "charge" α is given by

$$G(\phi t;\phi' t'=0) = \sum_m \frac{1}{2\pi}\exp(im(\phi-\phi'))\exp\left(-i\frac{\hbar}{2I}(m-\alpha\,\sigma_3)^2 t\right)$$

or

$$\exp\left(-i\frac{\hbar\alpha^2 t}{2I}\right)\sum_m \frac{1}{2\pi}\exp\left(im\left(\phi-\phi'+\sigma_3\frac{\hbar\, t\,\alpha}{I}\right)\right) \times \exp\left(-i\frac{\hbar\, m^2\, t}{2I}\right). \tag{104}$$

Now at the revival [43] time $t_N = \frac{4\pi I N}{\hbar}$, where N is an integer,

$$\begin{aligned} G(\phi\, t_N;\phi') &= \frac{1}{2\pi}\exp\left(-i\Delta\phi_N\frac{\alpha}{2}\right) \times \sum_m \exp(im(\phi-\phi'+\sigma_3\Delta\phi_N)) \\ &= \exp\left(-i\Delta\phi_N\frac{\alpha}{2}\right) \times \begin{pmatrix}\delta(\phi-\phi'+\Delta\phi_N) & 0\\ 0 & \delta(\phi-\phi'-\Delta\phi_N)\end{pmatrix} \end{aligned} \tag{105}$$

where $\Delta\phi_N = t_N\frac{\hbar\alpha}{I} = 4\pi N\alpha$. Thus an arbitrary initial, localized, wave packet is displaced, depending on its spin state, by an amount $\pm\Delta\phi_N$. Suppose $\alpha = m/p$ where m, p are integers, then the packet returns to its original starting point, i.e., $\Delta\phi = 0\,\mathrm{Mod}\,2\pi$ at t_{N^*} for $N^* = p$. So if a localized packet at $t = 0$ has the form

$$\psi(\phi, t=0) = \begin{pmatrix}\psi_u(\phi)\\ \psi_d(\phi)\end{pmatrix}, \tag{106}$$

it evolves to

$$\psi(\phi, t_{N^*}) = \exp(-iW_m(\alpha))\begin{pmatrix}\psi_u(\phi)\\ \psi_d(\phi)\end{pmatrix} \tag{107}$$

where

$$W_m(\alpha) \equiv \oint_m d\boldsymbol{R}\cdot\boldsymbol{A}_{AB}, \qquad \boldsymbol{A}_{AB} = \hat{\boldsymbol{\phi}}\frac{\alpha}{R} \tag{108}$$

is the argument of a Wilson loop integral with winding number m. Expression (107) demonstrates that an arbitrary wave packet revives, up to a topological phase factor $\exp(iW_m(\alpha))$, at its initial position. The latter demonstrates Abelian holonomy of the recurrence packet, a non-Abelian version of this phenomenon is presented elsewhere [44].

On a final note, at the time of writing I have become aware of recent literature in which similar themes, presented in this paper, are discussed. Synthetic gauge structures on a ring lattice have been explored in [45], and non-Abelian Wu-Yang structures have been observed in optical systems [46,47]. Non-Abelian gauge structures have also been recently investigated in condensed-matter systems [37,48,49].

ACKNOWLEDGMENTS

I wish to acknowledge support by the National Supercomputing Institute for use of the Intel Cherry-Creek computing cluster. Part of this work was also made possible by support from NSF, Quantum Leap Challenge Institute - Conceptualization Grant, initiative Grant No. 1936848.

APPENDIX A: THE SPIN-1/2 ROTOR—AN ANALYTIC TREATMENT

Hamiltonian (15) describes a neutral spin-1/2 particle constrained on a unit circle (i.e., a planar rotor with spin and moment of inertia I), subjected to the external magnetic field given by Eq. (3). The rotor coordinates $\phi = 0, 2\pi$ are identified. It can be rewritten as

$$\boldsymbol{H} = -\frac{1}{2I}\partial_\phi^2 + \boldsymbol{V}, \qquad \boldsymbol{V} = \begin{pmatrix}\Delta\cos\theta & -i\exp(-i\phi)\,\Delta\sin\theta\\ i\exp(i\phi)\,\Delta\sin\theta & -\Delta\cos\theta\end{pmatrix}. \tag{A1}$$

$\boldsymbol{H}$ commutes with

$$\boldsymbol{J} = -i\frac{\partial}{\partial\phi} + \frac{1}{2}\sigma_3, \tag{A2}$$

the eigenstates of which,

$$\psi = \begin{pmatrix}\exp(i(m-1)\phi)\,c_1\\ \exp(im\phi)\,c_2\end{pmatrix}, \tag{A3}$$

where m is an integer, satisfy

$$\boldsymbol{J}\psi = (m-1/2)\psi.$$

Using ansatz (A3) we find that the eigenvalue equation $(\boldsymbol{H}-E)\psi = 0$ reduces to

$$(\mathcal{H}-E)\underline{c} = 0$$

where $\underline{c} \equiv \binom{c_1}{c_2}$ and

$$\mathcal{H} = \left(\frac{m^2}{2I}+\frac{1-2m}{4I}\right)\mathbb{1} + \left(\frac{1-2m}{4I}+\Delta\cos\theta\right)\sigma_3 + \Delta\sin\theta\,\sigma_2. \tag{A4}$$

$\mathbb{1}$ is the unit matrix and σ_2, σ_3 are Pauli matrices. Introducing the unitary operator $\boldsymbol{W} = \exp(-i\sigma_1\Omega/2)$ where

$$\cos\Omega = \frac{\frac{(1-2m)}{4I}+\Delta\cos\theta}{\sqrt{\frac{(1-2m)^2}{16I^2}+\frac{(1-2m)\Delta\cos\theta}{2I}+\Delta^2}}, \qquad \sin\Omega = \frac{\Delta\sin\theta}{\sqrt{\frac{(1-2m)^2}{16I^2}+\frac{(1-2m)\Delta\cos\theta}{2I}+\Delta^2}}, \tag{A5}$$

we find that

$$\boldsymbol{W}\mathcal{H}\boldsymbol{W}^\dagger = \left(\frac{m^2}{2I}+\frac{1-2m}{4I}\right)\mathbb{1} + \sqrt{\Delta^2+\frac{(1-2m)^2}{16I^2}+\frac{(1-2m)\Delta\cos\theta}{2I}}\,\sigma_3. \tag{A6}$$

Therefore,

$$\psi_{\pm} = \begin{pmatrix} \exp(i(m-1)\phi) & 0 \\ 0 & \exp(im\phi) \end{pmatrix} \boldsymbol{W}^{\dagger} |\pm\rangle, \quad \text{(A7)}$$

where

$$|+\rangle = \begin{pmatrix} 1 \\ 0 \end{pmatrix} \quad |-\rangle = \begin{pmatrix} 0 \\ 1 \end{pmatrix} \quad \text{(A8)}$$

are eigenstates of $\boldsymbol{H}$. That is,

$$\boldsymbol{H}\psi_{\pm}(m) = E_{\pm}(m)\psi_{\pm}(m)$$

where

$$E_{\pm} = \frac{m^2}{2I} + \frac{(1-2m)}{4I} \pm \sqrt{\frac{(1-2m)^2}{16I^2} + \frac{(1-2m)\Delta\cos\theta}{2I} + \Delta^2}. \quad \text{(A9)}$$

In the limit $\Delta \to 0$, and for $1-2m > 0$, $\cos\Omega \to 1$,

$$\psi_+ \to \exp(i(m-1)\phi)|+\rangle, \quad E_+ \to \frac{(m-1)^2}{2I},$$
$$\psi_- \to \exp(im\phi)|-\rangle, \quad E_- \to \frac{m^2}{2I}, \quad \text{(A10)}$$

and likewise, for $1-2m < 0$ $\cos\Omega \to -1$,

$$\psi_+ \to \exp(im\phi)|+\rangle, \quad E_+ \to \frac{m^2}{2I},$$
$$\psi_- \to \exp(i(m-1)\phi)|-\rangle, \quad E_- \to \frac{(m-1)^2}{2I}. \quad \text{(A11)}$$

Equations (A10) and (A11) correspond to free rotor solutions.

In the limit $\Delta \to \infty$, provided that $\Delta > \frac{|1-2m|}{4I}$,

$$E_+(m) = m^2\left(\frac{1}{2I} + \frac{\sin^2\theta}{8I^2\Delta}\right) - m\left(\frac{(1+\cos\theta)}{2I} + \frac{\sin^2\theta}{8I^2\Delta}\right) + \Delta + \frac{1+\cos\theta}{4I} + \frac{\sin\theta^2}{32I^2\Delta} + \mathcal{O}\left(\frac{1}{\Delta^2}\right)\ldots \quad \text{(A12)}$$

and

$$E_-(m) = m^2\left(\frac{1}{2I} - \frac{\sin^2\theta}{8I^2\Delta}\right) - m\left(\frac{(1-\cos\theta)}{2I} - \frac{\sin^2\theta}{8I^2\Delta}\right) - \Delta + \frac{1-\cos\theta}{4I} - \frac{\sin\theta^2}{32I^2\Delta} + \mathcal{O}\left(\frac{1}{\Delta^2}\right)\ldots. \quad \text{(A13)}$$

APPENDIX B: PROPAGATOR FOR A SPIN-1/2 ROTOR COUPLED TO A WU-YANG FLUX TUBE

Consider the propagator for Schrödinger Eq. (35) in the region $|x_0| < 1$:

$$G(\phi\, t;\phi'\, t') \equiv \langle\phi|\exp(-iH\,\tau)|\phi'\rangle = \sum_m \psi'_m(E_+,\phi)\psi'^{\dagger}_m(E_+,\phi')\exp(-iE_+\tau) + \sum_m \psi'_m(E_-,\phi)\psi'^{\dagger}_m(E_-,\phi')\exp(-iE_-\tau) \quad \text{(B1)}$$

where $\tau = t - t' > 0$. Thus

$$G(\phi\, t;\phi'\, t') = \frac{1}{2\pi}\exp\left(-i\frac{\alpha^2}{2I}\tau\right)\exp(-i\Delta\sigma_3\tau) \times \sum_m \exp(i\,m(\phi-\phi'))\exp\left(-i\,\frac{m^2\tau}{2I}\right) \times \exp\left(-i\,\sigma_3\,m\,\frac{\alpha\tau}{I}\right). \quad \text{(B2)}$$

With the following definition of the Jacobi-theta function [50,51],

$$\theta_3(z,u) \equiv \sum_m \exp(i\pi m^2 u)\exp(2\,i\,m\,z), \quad \text{(B3)}$$

we reexpress

$$G(\phi\, t;\phi'\, t') \equiv \frac{1}{2\pi}\exp\left(-i\frac{\alpha^2\,\tau}{2I}\right)\exp(-i\Delta\sigma_3\tau) \times \begin{pmatrix} \theta_3(z_-,u) & 0 \\ 0 & \theta_3(z_+,u) \end{pmatrix} \quad \text{(B4)}$$

where

$$z_{\mp} = (\phi-\phi')/2 \mp \frac{\alpha\,\tau}{2I} \quad u = -\frac{\tau}{2\pi I}. \quad \text{(B5)}$$

Employing the identity [50]

$$\theta_3(z,u) = \frac{1}{\sqrt{-i\,u}}\exp\left(-i\frac{z^2}{\pi\,u}\right)\theta_3\left(-\frac{z}{u},-\frac{1}{u}\right) = \frac{\exp\left(\frac{-i\,z^2}{\pi\,u}\right)}{\sqrt{-i\,u}}\sum_m \exp\left(-\frac{i\pi\,m^2}{u}\right)\exp\left(\frac{2\,i\,m\,z}{u}\right) \quad \text{(B6)}$$

we rewrite (B4) as

$$G(\phi\, t;\phi'\, t') = \sqrt{\frac{I}{2\,\pi\,i\,\tau}}\exp(-i\sigma_3\Delta\tau) \times \sum_m \exp\left(iI\frac{(2m\pi-\phi+\phi')^2}{2\tau}\right) \times \exp(i\,\alpha(2m\pi-\phi+\phi')\,\sigma_3). \quad \text{(B7)}$$

APPENDIX C

According to Eqs. (60) and (61) the Schrödinger equation, in the adiabatic gauge, for a rotor with unit radius is

$$-\frac{1}{2I}\left(\frac{\partial}{\partial\phi} - i\boldsymbol{a}\right)^2 F + \Delta\sigma_3 F = i\frac{\partial F}{\partial t} \quad \text{(C1)}$$

where the gauge potential

$$\boldsymbol{a} = q\begin{pmatrix} \cos\theta & \exp(i\gamma)\sin\theta \\ \exp(-i\gamma)\sin\theta & -\cos\theta \end{pmatrix}, \quad \text{(C2)}$$

where q is an integer and θ, γ are parameters. To solve for its energy spectrum we let $F = \exp(im\phi)/\sqrt{2\pi}\,\boldsymbol{c}$ so that

$$\frac{(m\mathbb{1}-\boldsymbol{a})^2}{2\,I}\boldsymbol{c} + \sigma_3\Delta\,\boldsymbol{c} = i\dot{\boldsymbol{c}} \quad \text{(C3)}$$

or $\boldsymbol{h}\,\boldsymbol{c} = i\,\dot{\boldsymbol{c}}$:

$$\boldsymbol{h} = \mathbb{1}\frac{(m^2+q^2)}{2I} - \frac{m}{I}\begin{pmatrix} \cos\theta - \frac{I}{m}\Delta & \exp(i\gamma)\sin\theta \\ \exp(-i\gamma)\sin\theta & -\cos\theta + \frac{I}{m}\Delta \end{pmatrix} \tag{C4}$$

where we used the fact that $\boldsymbol{a}\cdot\boldsymbol{a} = q^2\,\mathbb{1}$. The eigenvalues of $\boldsymbol{h}$ are

$$\begin{aligned} e(m) &= e_0(m) \pm e_1(m), \\ e_0(m) &= \frac{m^2+q^2}{2I}, \\ e_1 &= \frac{\sqrt{m^2\,q^2 + I^2\,\Delta^2 - 2I\,m\,q\,\Delta\cos\theta}}{I} \end{aligned} \tag{C5}$$

and the partition function

$$\mathcal{Z} = 2\sum_m \exp(-\beta\, e_0(m))\cosh(\beta\, e_1(m)) \tag{C6}$$

where β is the inverse temperature. For $q = 1$, consider the limit $\Delta \ll 1$, in which

$$\begin{aligned} \mathcal{Z} \to 2\sum_m \exp\left(-\beta\,\frac{m^2+1}{2\,I}\right) \\ \times \cosh\left(\beta\left(\frac{m}{I} - \Delta\cos\theta\right)\right). \end{aligned} \tag{C7}$$

Using the Poisson summation formula, we find

$$\mathcal{Z} \to 2\sqrt{\frac{2\,\pi\,I}{\beta}}\sum_m \exp\left(-\frac{2\,I\,\pi^2\,m^2}{\beta}\right)\cosh(\beta\,\Delta\,\cos\theta). \tag{C8}$$

Thus, in this limit the partition function assumes the form of a free rotor in the presence of a constant "scalar" potential $\Delta\cos\theta$.

In the other extreme, $I\,\Delta \gg 1$,

$$\begin{aligned} \mathcal{Z} \to 2\sum_m \exp\left(-\beta\,\frac{m^2+1}{2\,I}\right) \\ \times \cosh\left(\beta\left(\Delta - \frac{m}{I}\cos\theta\right)\right) \end{aligned} \tag{C9}$$

or, applying the Poisson summation formula,

$$\begin{aligned} \mathcal{Z} \to 2\sqrt{\frac{2\,\pi\,I}{\beta}}\cosh(\beta\,\Delta)\exp\left(-\beta\frac{\sin^2\theta}{2\,I}\right) \\ \times\sum_m \exp\left(-\frac{2\,\pi^2\,m^2\,I}{\beta}\right)\cos(2\,\pi\,m\,\cos\theta). \end{aligned} \tag{C10}$$

In Fig. 13 we plotted the logarithm of the ratio $\mathcal{Z}/\mathcal{Z}_0$ where

$$\mathcal{Z}_0 \equiv 2\sqrt{\frac{2\,\pi\,I}{\beta}}\cosh(\beta\,\Delta)\exp\left(-\beta\frac{\sin^2\theta}{2\,I}\right).$$

In that figure the solid lines are calculated using the exact values Eq. (C6) for $\mathcal{Z}$, whereas the dashed lines represent the value obtained using the approximate expression (C10).

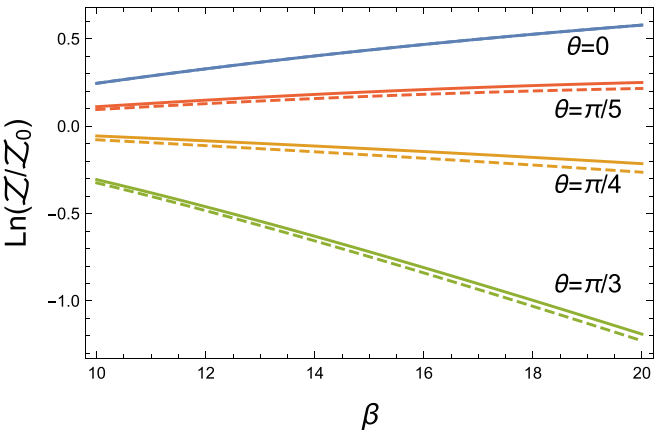

FIG. 13. Plot of ratio $Ln(\mathcal{Z}/\mathcal{Z}_0)$ as a function of the inverse temperature β. The dimensionless parameters $I = 1$, $\Delta = 100$.

According to Eq. (C10), the ratio

$$\mathcal{Z}/\mathcal{Z}_0 = \sum_m \exp\left(-\frac{2\,\pi^2\,m^2\,I}{\beta}\right)\cos(2\,\pi\,m\,\cos\theta)$$

in the limit $\beta \gg 1$. The variation of this ratio, shown in Fig. 13, demonstrates the role of the topological contribution $\cos(2\,\pi\,m\,\cos\theta)$ to the, gauge invariant, partition function.

APPENDIX D

According to Eq. (90) the reduced partition function

$$\begin{aligned} z &= 2\sum_m \exp(-\beta\, e_0)\cosh(\beta\, e_1), \\ e_0 &= \frac{m^2+\cos^2\theta}{2I}, \\ e_1 &= \sqrt{\Delta^2 + \frac{m^2}{I^2}\sin^2\theta}; \quad \Delta \equiv \frac{\sin^2\theta}{4I}. \end{aligned} \tag{D1}$$

At cold temperatures as, e.g., $\beta \to \infty$, the approximation

$$\begin{aligned} e_1 &\approx \alpha_0 + \alpha_1|m|, \\ \alpha_0 &= \Delta, \\ \alpha_1 &= -\Delta + \sqrt{\Delta^2 + \frac{\cos^2\theta}{I^2}} \end{aligned} \tag{D2}$$

is appropriate. Therefore, we need to evaluate

$$\begin{aligned} z = 2\sum_m \exp\left(-\beta\left(\frac{m^2+\cos^2\theta}{2I}\right)\right) \\ \times\cosh(\beta(\alpha_0 + |m|\alpha_1)) \end{aligned} \tag{D3}$$

or

$$\begin{aligned} z = 2\exp\left(-\beta\frac{\cos^2\theta}{2I}\right)\sum\exp\left(-\beta\frac{m^2}{2I}\right) \\ \times(\cosh(\beta\,\alpha_0)\cosh(\beta\,\alpha_1|m|) \\ +\ \sinh(\beta\,\alpha_0)\sinh(\beta\alpha_1|m|)). \end{aligned} \tag{D4}$$

Applying the Poisson summation formula to Eq. (D4) leads to

$$z = 2\exp\left(-\frac{\beta\,\cos^2\theta}{2I}\right)\sqrt{\frac{2\pi\,I}{\beta}}\Bigg(\cosh(\alpha_0\beta) \times \sum_k \exp\left(-\frac{2\,\pi^2\,I\,k^2}{\beta}\right)\exp\left(\frac{\alpha_1^2\,I\,\beta}{2}\right)\cos(2\,\pi\,I\,k\,\alpha_1) - \frac{2}{\sqrt{\pi}}\sinh(\alpha_0\,\beta)\sum_k \mathrm{Im}\,D_F\left(\sqrt{\frac{I}{2\beta}}(2\pi k - i\,\alpha_1\,\beta)\right)\Bigg) \tag{D5}$$

where D_F is the Dawson integral [52] and where the summation is over all integers k. It is useful to express the latter in terms of a confluent hypergeometric function [52]:

$$D_F(\xi) = \xi\,\exp(-\xi^2)\,{}_1F_1\left(\frac{1}{2},\frac{3}{2},\xi^2\right). \tag{D6}$$

For $|\xi| \gg 1$ we use the asymptotic expansion for the Kummer function [53]:

$${}_1F_1\left(\frac{1}{2},\frac{3}{2},\xi^2\right) \to \frac{\exp(\xi^2)}{2\xi^2} \pm \frac{i\sqrt{\pi}}{2\sqrt{\xi^2}} \tag{D7}$$

where the $\pm$ sign refers to the cases

$$-\frac{\pi}{2} < \arg(\xi^2) < \frac{3\pi}{2} \quad \text{and} \quad -\frac{3\pi}{2} < \arg(\xi^2) \leqslant -\frac{\pi}{2},$$

respectively. Or

$$D_F(\xi) \to \frac{1}{2\,\xi} \pm \frac{i\sqrt{\pi}}{2}\,\exp(-\xi^2) \tag{D8}$$

where $\pm$ corresponds to $\mathrm{Re}(\xi) > -\mathrm{Im}(\xi)$ and $\mathrm{Re}(\xi) < -\mathrm{Im}(\xi)$, respectively. Since $\xi = \sqrt{\frac{I}{2\beta}}\,(2\pi\,k - i\,\beta\,\alpha_1)$ we find that as $\beta \to \infty$ ($\alpha_1 \neq 0$)

$$\mathrm{Im}\,D_F\left(\sqrt{\frac{I}{2\beta}}(2\pi k - i\,\alpha_1\,\beta)\right) \to \sqrt{\frac{\beta}{2\,I}}\,\frac{\beta\,\alpha_1}{4\pi^2k^2 + \alpha_1^2\beta^2} \pm \frac{\sqrt{\pi}}{2}\exp\left(\frac{\alpha_1^2\,I\,\beta}{2}\right)\exp\left(-\frac{2\pi^2\,I\,k^2}{\beta}\right)\cos(2\pi\,I\,k\,\alpha_1). \tag{D9}$$

Thus, if $\alpha_1 > 0$,

$$z \approx \sqrt{\frac{2\pi\,I}{\beta}}\exp\left(-\frac{\beta\,\cos^2\theta}{2I}\right)\exp(\alpha_0\,\beta)\exp\left(\frac{\alpha_1^2\,I\,\beta}{2}\right) \times \sum_k \exp\left(-\frac{2\pi^2 I\,k^2}{\beta}\right)\cos(2\pi\,I\,\alpha_1\,k)\,g(k) \tag{D10}$$

where

$$g(k) = 2 \quad \text{for} \quad 2\pi\,k < \alpha_1\,\beta,$$
$$g(k) = 0 \quad \text{for} \quad 2\pi\,k > \alpha_1\,\beta$$

and we used the fact that

$$\sum_k \frac{\alpha_1\beta}{4\,\pi^2\,k^2 + \alpha_1^2\beta^2} = \frac{1}{2}\coth\frac{\alpha_1\,\beta}{2} \approx \frac{1}{2} \tag{D11}$$

in this limit. Using definitions (D2) we find that

$$z \to 2\sqrt{\frac{2\,\pi I}{\beta}}\,\exp(\beta\,V(\theta)) \times \sum_k \exp(-S_0(k))\cos(2\,\pi\,k\,\Omega) \tag{D12}$$

where $S_0(k)$ is the Wick rotated action for a planar rotor undergoing k circuits and

$$V(\theta) = -\frac{\cos^2\theta}{I} + \alpha_0 + \frac{I\,{\alpha_1}^2}{2},$$
$$\Omega = -\frac{\sin^2\theta}{4} + \sqrt{\frac{\sin^2\theta}{16} + \cos^2\theta}. \tag{D13}$$

[1] A. Aharonov and D. Bohm, Phys. Rev. **115**, 485 (1959).
[2] P. Ball, *Beyond Weird* (University of Chicago, Chicago, 2018).
[3] R. Feynman, R. Leighton, and M. Sands, *The Feynman Lectures on Physics, Vol. III: The New Millennium Edition: Quantum Mechanics*, The Feynman Lectures on Physics (Basic Books, New York, 2011).
[4] A. Peruzzo, P. Shadbolt, N. Brunner, S. Popescu, and J. L. O'Brien, Science **338**, 634 (2012).
[5] Y.-H. Kim, R. Yu, S. P. Kulik, Y. Shih, and M. O. Scully, Phys. Rev. Lett. **84**, 1 (2000).
[6] D. J. Thouless, M. Kohmoto, M. P. Nightingale, and M. den Nijs, Phys. Rev. Lett. **49**, 405 (1982).
[7] F. Wilczek, Phys. Rev. Lett. **49**, 957 (1982).
[8] M. Z. Hasan and C. L. Kane, Rev. Mod. Phys. **82**, 3045 (2010).
[9] S. D. Sarma, M. Freedman, and C. Nayak, Phys. Today **59**(7) 32 (2006).
[10] J. Preskill, arXiv:quant-ph/9712048 (1997).
[11] T. T. Wu and C. N. Yang, Phys. Rev. D **12**, 3845 (1975).
[12] P. A. Horváthy, Phys. Rev. D. **33**, 407 (1986).
[13] P. A. M. Dirac, Proc. R. Soc. A **133**, 60 (1931).
[14] K. Jiménez-Garcia, L. J. LeBlanc, R. A. Williams, M. C. Beeler, A. R. Perry, and I. B. Spielman, Phys. Rev. Lett. **108**, 225303 (2012).
[15] C. A. Mead and G. D. Truhlar, J. Chem. Phys. **70**, 2284 (1979).
[16] J. Moody, A. Shapere, and F. Wilczek, Phys. Rev. Lett. **56**, 893 (1986).
[17] B. Zygelman and A. Dalgarno, Phys. Rev. A **33**, 3853 (1986).
[18] B. Zygelman, Phys. Lett. A **125**, 476 (1987).
[19] S. K. Min, A. Abedi, K. S. Kim, and E. K. U. Gross, Phys. Rev. Lett. **113**, 263004 (2014).
[20] C. A. Mead, Chem. Phys. **49**, 23 (1980).
[21] B. Zygelman, J. Phys. B **50**, 025102 (2016).

[22] B. K. Kendrick, J. Chem. Phys. **148**, 044116 (2018).
[23] D. Yuan, Y. Guan, W. Chen, H. Zhao, S. Yu, C. Luo, Y. Tan, T. Xie, X. Wang, Z. Sun, D. H. Zhang, and X. Yang, Science **362**, 1289 (2018).
[24] J. March-Russell, J. Preskill, and F. Wilczek, Phys. Rev. Lett. **68**, 2567 (1992).
[25] Y. Mankeenko, Phys. Atom. Nucl. **73**, 878 (2010).
[26] R. Jackiw, Comments At. Mol. Phys. **21** 71 (1988).
[27] B. Zygelman, Phys. Rev. Lett. **64**, 256 (1990).
[28] B. Zygelman, Phys. Rev. A **92**, 043620 (2015).
[29] F. Wilczek and A. Zee, Phys. Rev. Lett. **52**, 2111 (1984).
[30] M. V. Berry, in *Geometric Phases in Physics*, edited by A. Shapere and F. Wilczek (World Scientific, Singapore, 1989), p. 1.
[31] M. R. Hermann and J. A. Fleck, Phys. Rev. A **38**, 6000 (1988).
[32] B. Zygelman, Phys. Rev. A **86**, 042704 (2012).
[33] A. Bhattacharyya, Bull. Calcutta Math. Soc. **35**, 99 (1943).
[34] The Wilson loop integral for a WY flux tube is twice that of a single AB flux tube.
[35] P. Dirac, *Lectures on Quantum Mechanics*, Belfer Graduate School of Science, Monograph Series (Dover, New York, 2001).
[36] A. Scardicchio, Phys. Lett. A **300**, 7 (2002).
[37] T. Holder, D. Kaplan, and B. Yan, Phys. Rev. Research **2**, 033100 (2020).
[38] M. V. Berry, Proc. R. Soc. A **392**, 45 (1984).
[39] E. Cohen, H. Larocque, F. Bouchard, F. Nejadsattari, Y. Gefen, and E. Karimi, Nat. Rev. Phys. **1**, 437 (2019).
[40] M. Born and K. Huang, *Dynamical Theory of Crystal Lattices* (Oxford University, New York, 1954).
[41] N. F. Mott and H. S. W. Massey, *The Theory of Atomic Collisions*, 2nd ed. (Oxford University, New York, 1949), p. 128.
[42] E. Urban, N. Glikin, S. Mouradian, K. Krimmel, B. Hemmerling, and H. Haeffner, Phys. Rev. Lett. **123**, 133202 (2019).
[43] R. Robinett, Phys. Rep. **392**, 1 (2004).
[44] B. Zygelman (unpublished).
[45] K. K. Das and M. Gajdacz, Sci. Rep. **9**, 14220 (2019).
[46] Y. Yang, C. Peng, D. Zhu, H. Buljan, J. D. Joannopoulos, B. Zhen, and M. Soljačić, Science **365**, 1021 (2019).
[47] Y. Chen, R.-Y. Zhang, Z. Xiong, Z. H. Hang, J. Li, J. Q. Shen, and C. T. Chan, Nat. Commun. **10**, 3125 (2019).
[48] K. Snizhko, R. Egger, and Y. Gefen, Phys. Rev. Lett. **123**, 060405 (2019).
[49] K. Snizhko, R. Egger, and Y. Gefen, Phys. Rev. B **100**, 085303 (2019).
[50] R. Bellman, *A Brief Introduction to Theta Functions* (Dover, New York, 2013).
[51] L. Schulman, *Techniques and Applications of Path Integration* (Dover, New York, 2005).
[52] V. Nijimbre, J. Appl. Anal. Comput. **25**, 179 (2019).
[53] M. Abramowitz and I. A. Stegun, *Handbook of Mathematical Functions with Formulas, Graphs, and Mathematical Tables* (Dover, New York, 1964).